

A ground–based proper motion study of twelve nearby Globular Clusters

W. Narloch¹★, J. Kaluzny[†], R. Poleski², M. Rożyczka¹, W. Pych¹, I. B. Thompson³

¹*Nicolaus Copernicus Astronomical Center, of the Polish Academy of Sciences, ul. Bartycka 18, 00-716 Warsaw, Poland*

²*Department of Astronomy, Ohio State University, 140 West 18th Avenue, Columbus, OH 43210, USA*

³*The Observatories of the Carnegie Institution of Washington, 813 Santa Barbara Street, Pasadena, CA 91101, USA*

Accepted XXX. Received YYY; in original form ZZZ

ABSTRACT

We derive relative proper motions of stars in the fields of the globular clusters M12, NGC 6362, M4, M55, M22, NGC 6752, NGC 3201, M30, M10, NGC 362, M5, and 47 Tucanae based on data collected between 1997 and 2015 with the 1-m Swope telescope of Las Campanas Observatory. We determine membership class and membership probability for over 446 000 objects, and show that these are efficient methods for separating field stars from members of the cluster. In particular, membership probabilities of variable stars and blue/yellow/red stragglers are determined. Finally, we find absolute proper motions for six globular clusters from our sample: M55, NGC 3201, M10, NGC 362, M5, and 47 Tuc. An electronic catalogue of the derived proper motions is publicly available via the internet.

Key words: globular clusters: individual: M12, NGC 6362, M4, M55, M22, NGC 6752, NGC 3201, M30, M10, NGC 362, M5, 47 Tucanae – astrometry – blue stragglers

1 INTRODUCTION

Globular clusters (GCs) are important laboratories to study both stellar evolution and dynamics as well as chemical evolution of the universe. The analysis presented in this work is a part of the CASE project (Cluster AgeS Experiment, Kaluzny et al. 2005) which is devoted to a search for and follow-up observations of variable stars in the fields of nearby GCs, in particular, for detached eclipsing binaries which might be useful in determining distances and ages of GCs (e.g. Thompson et al. 2010). An additional result of the project is the discovery of a large number of previously unknown variable stars of other types found in the fields of the GCs, for example RR Lyrae stars which might be interesting for astroseismic studies (Smolec et al. 2017). But to fully benefit such studies of the properties of GCs, it is important to separate members of the clusters from field stars. Reliable separation can be achieved, e.g., by a proper motion (PM) study.

The first PM measurements in GCs were made using photographic plates (Ebbighausen 1942; Cudworth 1980, and references therein). Later studies replaced the photo-

graphic plates with CCD detectors. The CCD data allowed a significant reduction in the level of statistical uncertainties and permitted reliable results to be obtained for a larger number of fainter stars even with a short time base of only a few years (Anderson et al. 2006; Bellini et al. 2009).

The launch of the Hubble Space Telescope (HST) enabled studies of dense central parts of GCs, and PM measurements of stars with a high accuracy (tens of $\mu\text{as}/\text{yr}$ for the brightest stars). Such precision is crucial in, e.g., studies of internal kinematics of GCs (e.g. Watkins et al. 2015).

The GAIA space mission is expected to provide astrometry for about 1 billion point sources down to $V \approx 20$ mag with precision of tens of μas or better for objects brighter than $V \approx 15$ mag, and radial velocities down to $V \approx 17$ mag (Mignard 2005; Pancino et al. 2013, 2017). It aims to chart a three-dimensional map of the Milky Way out to a distance of ≈ 8.5 kpc from the Sun including fields of all GCs considered in this work. The first data release occurred last year (Lindegren et al. 2016), and contained high-accuracy positions for more than 1 billion stars brighter than $V \approx 21$ mag. This limit is still about one magnitude shallower than what we have obtained in this work. We have thus been able to measure more stars than GAIA in the fields of our sample of GCs (especially close to the cluster center).

At this moment, GAIA PMs have been provided for only the brightest stars. This is in common with the Hipparcos and Tycho-2 catalogues, which omit the fields of GCs.

★ E-mail: wnarloch@camk.edu.pl (WN); mnr@camk.edu.pl (MR); poleski.1@osu.edu (RP); pych@camk.edu.pl (WP); ian@obs.carnegiescience.edu (IBT)

† Deceased

This is a distinct advantage of our catalogue comparing to the first release of the GAIA catalogue. The expected final accuracy of GAIA PMs for GC members, ≈ 1 mas/yr at $V \approx 21$ mag, is comparable to ours (see Section 3.2). For brighter stars GAIA measurements will be more accurate (e.g. ≈ 20 vs. ≈ 60 $\mu\text{as}/\text{yr}$ at $V \approx 15$ mag); however the final accuracy is unlikely to be reached before 2020, and only the latest few Gaia releases (2020–2023) are expected to provide a significant breakthrough in GC research (Pancino et al. 2017).

In this paper we present studies of relative proper motions of stars in the fields of twelve nearby galactic GCs: M12, NGC 6362, M4, M55, M22, NGC 6752, NGC 3201, M30, M10, NGC 362, M5, and two fields (East and West) of 47 Tuc. Previous analyses of observations of the first six GCs was published by Zloczewski et al. (2011, 2012) and for M55 by Sariya et al. (2012). In the first two papers the authors used data from 2.5 m du Pont telescope with a field of view of 8.83×8.83 arcmin². Although they obtained reliable PMs and membership status for stars close to the center of the cluster, these studies lack information about PMs of more distant objects. Data for the third paper were collected with the Wide Field Camera (WFI) mounted on the 2.2 m MPG/ESO telescope. The authors created a membership probability catalogue in a wide field (26×22 arcmin²), however the faintest stars they measured were no fainter than ≈ 20 mag in V -band, compared to ≈ 21.5 mag in the present work. In addition, the camera had some gaps between CCD chips, and so objects located in these regions were not measured. A PM catalogue for M10 based on photographic plates and Hipparcos data was presented by Chen et al. (2000), where they provided absolute PMs for 532 stars. The recent study of Cioni et al. (2016) resulted in a catalogue of absolute PMs in 47 Tuc based on VISTA data. With a time baseline of just 1-yr they measured PMs of about 86 000 stars located 10–60 arcmin from the cluster center, preferentially in the direction to the Small Magellanic Cloud (SMC, i.e. in a field partially covering that of ours). Extensive studies of PMs in GCs from our list have also been made with the HST, e.g., Drukier (2003, for NGC 6752), McLaughlin et al. (2006, for 47 Tuc), Bellini et al. (2014, in regions of 22 galactic GCs) or Simunovic et al. (2016, for 38 galactic GCs). HST data provide deep and precise photometry for thousands of stars impossible to resolve with ground-based telescopes, but the data cover a field of view of only about 3×3 arcmin², which is much smaller than in the present analysis. Thus, in many aspects, the work presented here is a valuable supplement to the surveys quoted above.

The absolute PMs of GCs are important quantities, which when combined with radial velocities of the systems allow a derivation of the space motions of GCs. Knowledge of the latter helps to build dynamical models of the Galaxy, trace the gravitational potential of the Galaxy, or find the origin of the GCs themselves. Presently, for each GC considered in this work, there are at least a few measurements of absolute PMs. The earliest results for all our GCs but one are summarized in Dinescu et al. (1999), later calculations come from e.g. Chen et al. (2000); Dambis (2006); Casetti–Dinescu et al. (2007) or Zloczewski et al. (2011). Only 47 Tuc has several measurements (except already cited, also Freire et al. 2001, 2003; Anderson et al. 2003). The newest ones come from Cioni et al. (2016) and Watkins et al. (2016). However,

all these determinations are based on different methods, and produce different results. For this reason it is valuable to make additional independent measurements, which is what we have done in the present work.

The paper is organized as follows. In Section 2 we describe observational data selection and reduction. Procedures employed for measuring PMs and calculating membership probabilities of individual stars are discussed in Section 3. Section 4 contains color–magnitude diagrams (CMDs) for the analyzed cluster fields. In Section 5 we derive absolute PMs for six GCs from our sample, and Section 6 provides a brief summary of the paper.

2 DATA SELECTION AND PREPARATION

The images analyzed in this paper were collected within the CASE project between the years 1997–2015. Observations in V and B filters were obtained using the 1-m Swope telescope located at Las Campanas Observatory in Chile. Two CCD cameras were used: SITE#3 with a field of view of 14.8×22.8 arcmin² and a scale of 0.435 arcsec/pixel during years 1997–2010 and E2V CCD231-84 with a field of view of 29.7×29.8 arcmin² and the same pixel scale in 2015. Equatorial coordinates of the field centers of the reference images are listed in Tab. 1.

The CASE project was not designed for astrometry purposes and in order to save CCD readout time a subraster was often used. As a result the final field sizes of our data sets were not uniform. As a consequence, the PM errors are larger for stars located close to the edge of a reference image, because of the smaller number of epochs used in the calculations. Tab. 2 contains information about our data sets.

2.1 Data reduction

For each GC reference images in both V and B filters were prepared. These were used for CMD construction and compilation of a list of reference stars (hereafter: master list). The reference images were selected to have the best possible quality and to cover the widest possible field of view. To that end, we chose a few to several best images obtained consecutively during one night with the same exposure time, low air masses, and background, and stacked them into one averaged image using the Difference Image Analysis PL (DIAPL) package¹. The number of stacked images varied from 7 to 18 in the V filter and from 4 to 8 in the B filter (in the case of M5 only a single exposure in the B filter was used). The stacked images were cleaned of cosmic rays and bad pixels, and have a significantly higher signal to noise ratio than any single exposure. To reduce the effects of PSF variability, each reference image was divided into overlapping subframes (usually 24 but in the case of M30 and NGC 362, which are strongly concentrated, only 6), which were analyzed independently. Profile photometry for each subframe was measured with the DAOPHOT/ALLSTAR package (Stetson 1987) assuming a Gaussian function with spatial variability to characterize the PSF. Because of crowding, master lists were obtained

¹ Originally written by Wozniak (2000) and developed by W. Pych. Available at <http://users.camk.edu.pl/pych/DIAPL/>

Table 1. Equatorial and galactical coordinates of the centers of reference images.

Field	Messier	$\alpha_{2000}[^{\circ}]$	$\delta_{2000}[^{\circ}]$	$l[^{\circ}]$	$b[^{\circ}]$
NGC 6218	M12	251.824072	-1.984139	15.69008	26.28193
NGC 6362		262.982455	-67.032649	325.56947	-17.56350
NGC 6121	M4	245.911419	-26.524932	350.98267	15.96286
NGC 6809	M55	294.999089	-30.963256	8.79412	-23.27151
NGC 6656	M22	279.103212	-23.913256	9.88592	-7.55835
NGC 6752		287.712680	-59.985725	336.49111	-25.62647
NGC 3201		154.400593	-46.411364	277.22645	8.64011
NGC 7099	M30	325.117975	-23.180452	27.18754	-46.85866
NGC 6254	M10	254.290704	-4.100178	15.13883	23.07343
NGC 362		15.818869	-70.849659	301.52851	-46.24641
NGC 5904	M5	229.649514	2.079606	3.86727	46.78676
NGC 104 E	47 Tuc E	6.372329	-72.086153	305.74390	-44.90031
NGC 104 W	47 Tuc W	5.661052	-72.085975	306.04922	-44.86778

iteratively, gradually decreasing the detection threshold. In the final iteration the images were examined by eye and stars omitted in the automatic procedure were added manually. In the end, aperture corrections, obtained for each subframe separately using the DAOGROW package (Stetson 1990), were applied. Instrumental CMDs were then derived from these photometry files.

PMs were calculated based on individual images in the V -filter selected from among all available exposures of a given cluster (see Table 2). For further analysis frames characterized by seeing ranging from ≈ 1.17 to ≈ 1.52 arcsec (slightly larger only for 47 Tuc), the lowest possible background, and air mass lower than 1.45 were used. The latter constraint is a compromise between minimizing refraction effects and choosing the maximal number of single frames used for the calculations. These were then divided into the same number of subframes as the corresponding reference images.

Subsequently, stars from the reference lists were identified in each subframe of a given cluster, and profile photometry was measured with the ALLSTAR parameter REDET set to 1, enabling a re-determination of star coordinates.

2.2 Photometric calibration

Instrumental CMDs for nine clusters (M12, NGC 6362, M4, M55, M22, NGC 6752, NGC 3201, M5 and 47 Tuc) were calibrated using linear transformations to already existing standard CMDs for these clusters (Mazur et al. 2003; Kaluzny et al. 2013a, 2015a,b). The transformations followed:

$$\begin{aligned}
 v &= V + a_1 + a_2(B - V) \\
 b &= B + b_1 + b_2(B - V) \\
 b - v &= c_1 + c_2(B - V)
 \end{aligned}
 \tag{1}$$

where v , b and $b - v$ are instrumental and V , B and $B - V$ are standard magnitudes and colors, respectively, and a_1 , a_2 , b_1 , b_2 , c_1 and c_2 are transformation coefficients. Calibration of M10 was based on 24 Landolt standards (Landolt 1992) observed within the CASE project with the Swope telescope and SITE#3 camera in five Landolt fields on May 29th 1998. M30 and NGC 362 were calibrated on a base of 45 standard stars from three Landolt fields observed on Aug 6th 2000.

3 PROPER MOTIONS

3.1 Measurements

The procedure employed to derive relative PMs was similar to that of Anderson et al. (2006) (also described in Zloczewski et al. 2011, 2012), in which positions of stars in different epochs are determined with respect to nearby cluster members. This is the so called *local transformation method*. Before attempting the measurements, we removed stars with relatively large magnitude errors (σ_V) from the lists of profile photometry. The following procedure was used: (i) a curve of the form $f = a \cdot \exp(V) + b$ was fitted to magnitude–magnitude error relation, where a , b are fitting parameters, (ii) for every subframe a magnitude V_S was selected such that for $V < V_S$ stars located above the curve were rejected, (iii) for $V > V_S$ stars with $\sigma_V > 1.3f$ were rejected. Next, from the master list we selected candidates for *grid stars* which were used as stable points for geometrical transformations between subframes.

As a first guess we selected stars located on main sequence (MS) and red giant branch (RGB) of the cluster’s CMD. Those on the blue part of the horizontal branch (HB) had to be excluded because of *differential chromatic refraction* (DCR) which causes relative shifts in positions of stars of different colors (e.g. Anderson et al. 2006). To that end, a simple color criterion would be sufficient. However, CMDs of some clusters (e.g. M4, M22 or NGC 6362) contain appreciable numbers of stars located to the left of the RGB and above the subgiant branch (SGB), most of which must be field interlopers. In such cases, employing a color criterion would contaminate the first-guess grid sample. To avoid this, we applied the above population criterion instead, and, as a consequence, red HB stars were lost from the grid sample. However, since in all clusters they are a minute fraction (≤ 0.03) of the MS/SGB/RGB population, excluding them had practically no effect on the results.

The photometric quality of grid candidates was estimated based on the values of the CHI and SHARP parameters returned by ALLSTAR. As in Zloczewski et al. (2012), only stars with $0.02 \leq CHI \leq 1.00$ and $-0.3 \leq SHARP \leq 0.3$ were included. To each star, grid stars located in a circle with a radius of 150 pixels (≈ 1.09 arcmin) centered on that star were assigned. If there were fewer than 40 stars inside the circle, the radius was successively increased by 50 pixels

Table 2. Information about data sets used for PM calculations.

Field	number of epochs	number of frames	time span between first and last epoch [yr]	mean FWHM [arcsec]	standard deviation of mean FWHM [arcsec]
M12	8	779	9.12	1.31	0.11
NGC 6362	11	1233	10.40	1.39	0.12
M4	11	1640	11.06	1.32	0.14
M55	12	2141	12.37	1.40	0.18
M22	5	1254	8.35	1.32	0.11
NGC 6752	3	405	12.32	1.38	0.10
NGC 3201	6	579	11.21	1.32	0.11
M30	2	531	14.98	1.31	0.10
M10	3	764	17.06	1.31	0.10
NGC 362	13	1119	17.94	1.43	0.11
M5	8	770	18.12	1.37	0.12
47 Tuc E	10	1019	16.87	1.54	0.16
47 Tuc W	8	749	10.84	1.58	0.15

(≈ 0.36 arcmin) until this condition was fulfilled. The number of grid stars ranged from a few tens to a few hundreds per star. For each star, a local geometrical transformation was found between the positions of grid stars on the reference frame and their positions on each single frame of a given cluster. To that end, we used two-dimensional 3rd order Chebyshev polynomials available in IRAF² tasks *immatch.geomap* and *immatch.geoxytran*.

Subsequently, coordinates (X_R, Y_R) of a given star on the reference image were transformed into expected coordinates (X_C, Y_C) of this star, and then relative motions were derived as a difference between expected and observed positions $\Delta X = X_C - X_O$ and $\Delta Y = Y_C - Y_O$. Finally, PMs μ_X and μ_Y were derived from weighted linear least-square fits to ΔX and ΔY as functions of time. The weight of a point was defined as the square root of the sum of squared uncertainties of the grid transformation (returned by IRAF task *immatch.geomap*) and the PSF fitting (Kuijken et al. 2002). The fitting was attempted for objects with positions measured in at least three epochs spanning at least three years except for stars in M30 (see Table 2). Confidence level was set to 99%, i.e., only results with significance of the fit greater than that value were considered as reliable measurements. Fig. 1 shows an example of fitting for the star #150770 from M4.

PM calculations were conducted in three steps. First, we determined PMs of grid stars. Whenever it was necessary, stars with large PMs were rejected, and this step was repeated. That happened when fast moving field stars were significantly affecting the transformation between frames. In the next step we calculated PMs for all stars in the field of a given cluster basing on the new grid stars. Finally, we again selected new grid candidates from all stars (keeping the conditions described above) and repeated the last step. Such a procedure allowed to minimize the effect of grid star motions.

² IRAF (Image Reduction and Analysis Facility) is distributed by the National Optical Astronomy Observatories, operated by Association of Universities for Research in Astronomy (AURA), Inc., under cooperative agreement with the National Science Foundation (NSF).

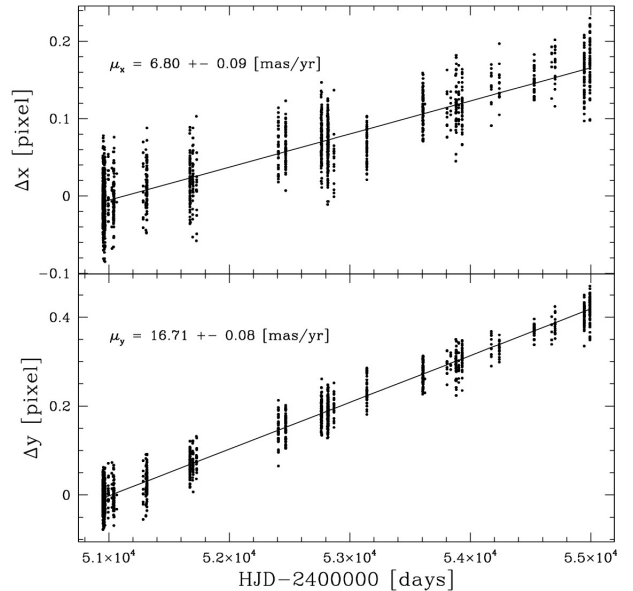


Figure 1. An example of the PM determination of star #150770 from M4 with $V = 18.149$ mag. Proper motion is the slope of the linear fit to Δx and Δy versus time. The Δx and Δy are differences between reference position of a given star and position measured at given epoch.

Table 3 summarizes the number of stars for which PMs were obtained.

Equatorial coordinates of the measured stars were derived from an astrometric solution based on stars with $V < 17$ mag from the Fourth U. S. Naval Observatory CCD Astrograph Catalog (UCAC4, Zacharias et al. 2012). The average residual of the solution ranged from $0.''13$ for M22 to $0.''29$ for NGC 6752. Translation from (μ_x, μ_y) to $(\mu_\alpha \cos \delta, \mu_\delta)$ was based on the same astrometric solution.

Table 3. Number of stars with measured PMs.

Field	number
M12	19120
NGC 6362	21851
M4	24304
M55	39566
M22	87030
NGC 6752	37454
NGC 3201	32795
M30	12638
M10	27895
NGC 362	23879
M5	37042
47 Tuc E	42506
47 Tuc W	43161

3.2 Error discussion

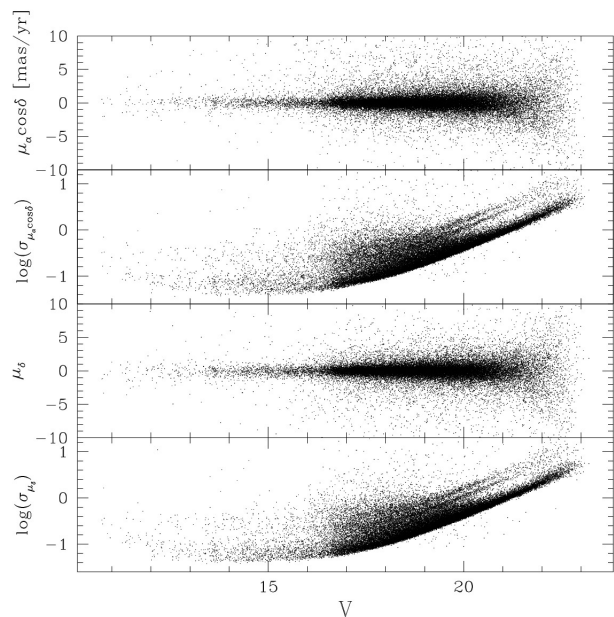
PM errors given in the catalogue are statistical errors calculated from linear fitting. The errors depend on the following effects:

- 1) decreasing signal to noise ratio for fainter stars,
- 2) location of the star on the image (stars located close to the edges of the frame have smaller numbers of grid candidates and noticeably larger PM uncertainties),
- 3) frequency of blending (blends are more likely for stars located closer to the center of a cluster, and for clusters at larger heliocentric distances),
- 4) uncertainties of transformations between images,
- 5) number of epochs and total number of exposures used for calculations,
- 6) time span between first and last epoch,
- 7) DCR effect.

The relevance of the first three effects is illustrated in Fig. 2 for the example of NGC 6752. Characteristic is the growth of uncertainties for fainter stars, which is a direct consequence of item 1). For red giants and horizontal branch stars the median of the uncertainties in both coordinates ranged from 0.04 mas/yr in M4 to 0.25 mas/yr in 47 Tuc W. For subgiants (SG) and stars located in the vicinity of the main sequence turn off point (MSTO) these values ranged from 0.05 mas/yr in M4 to 0.38 mas/yr in 47 Tuc W, and for stars from the lower MS - from 0.12 mas/yr to 0.92 mas/yr, respectively. The two weak branches visible in panels 2 and 4 of Fig. 2 for $V > 20$ mag are populated by stars from the edges of the reference image. The distance between these and the main branch is a measure of the combined inaccuracies related to item 2) and to the fact that fewer epochs were available for these objects. Finally, points spread at the center of the plot ($15.5 < V < 19$) mag are stars from the crowded center of the cluster, whose PM errors are mainly caused by blending.

The uncertainty of the transformations varies depending on star and epoch, and is a complex combination of the employed formulae and the quality of the data to be transformed, which in turn depends on effects 1)–3). Its magnitude can be assessed from the vertical spread of points representing measurements in a given epoch (see Figure 1 for an example).

Points 4) and 5) are discussed below for the example of


Figure 2. Plots of PMs and log of their uncertainties for NGC 6752.

47 Tuc. A total of 2888 stars were measured independently in the overlapping part of the E and W fields of this cluster, a strip 300 pixels (2.175 arcmin) wide. Note that we compare stars, first, located close to the edges of the subframes and second, from the vicinity of the cluster center. In both cases PM uncertainties are larger than elsewhere in the field. For this reason, we calculated the average PM differences in right ascension and declination for stars with PM uncertainties lower than 10 mas/yr (2712 stars) only. The means were then 0.469 ± 2.254 mas/yr and 0.141 ± 2.194 mas/yr. After applying σ -clipping at the level of 3σ these values are equal to 0.374 ± 2.03 mas/yr and 0.179 ± 2.0 mas/yr. If we assume that PM uncertainties in the E and W fields can be expressed as $\frac{\epsilon}{\Delta t \sqrt{N}}$, where Δt is the time base and N is number of epochs used for PM determination in a given field (see Table 2), then by calculating the sum of their squares and assuming that it is equal to square of the uncertainty (2 mas/yr obtained above), we can obtain ϵ . Then, by applying the above formula with known ϵ the average PM uncertainties are ≈ 1.0 mas/yr and ≈ 1.7 mas/yr for the E and W fields, respectively. This means that the PM measurements in the E field are on average by 0.7 mas/yr more accurate than in W. The difference of PM quality between these two fields comes mainly from field W. It has fewer epochs than for field E, and, even more importantly, the time span between the first and the last epoch was shorter by six years (see Table 2).

Refraction affects the data in two ways. Firstly, by modifying (x,y) coordinates of stars with the same color by amounts depending on the air mass at the position of a given star. This effect is minimized by the local transformation method we apply in the present survey. Secondly, via the DCR effect mentioned above. The DCR increases the spread of points in a single epoch, and may cause systematic shifts in PMs of stars with different colors. To assess its importance, we made linear fits to the relations between

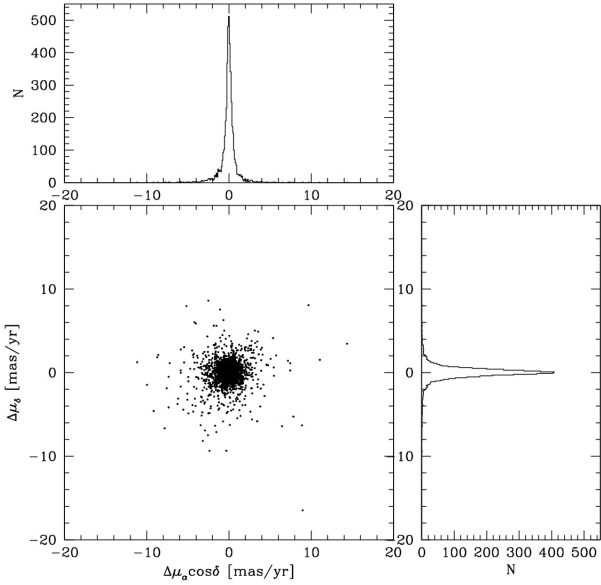


Figure 3. Differences between PMs of common stars from overlapping subframes in M4. *Panels:* VPD of the PM differences (*lower left*); marginal histogram of differences in right ascension, where N are counts (*upper left*); marginal histogram of differences in declination (*right*).

Δx and Δy and air mass for one of the bluest ($B - V = -0.028$ mag) and one of the reddest ($B - V = 0.757$ mag) stars in NGC 6752 which has a relatively strong blue HB. For the red star, no significant deviations from zero were observed for the whole air mass range. For the blue star, at the largest air mass of 1.45 the deviation amounted to ≈ 0.06 px, which was significantly less than the Δx or Δy spread at any epoch. Moreover, about 80% of the images were taken at air masses smaller than ≈ 1.3 , at which the deviation was still at least two times smaller. We concluded that small systematic PM errors were likely for blue HB stars only, and did not attempt to introduce any corrections.

The overall consistency of the measurements was verified by comparing PMs of stars from overlapping parts of the subframes (where each star was measured independently at least two times). An example comparison is shown in Fig. 3. The symmetry of the Vector Point Diagram (VPD) indicates that the differences are random. Also, the marginal distributions take a Gaussian shape which further confirms this conclusion. Average PM differences depend on subframes taken for the comparison, but all of these are equal to zero within the errors. After rejecting outliers, the average differences ($\Delta\mu_\alpha \cos \delta, \Delta\mu_\delta$) between stars from overlapping regions of the four center subfields are $(-0.07 \pm 1.14, 0.06 \pm 1.16)$ mas/yr, between those of the twelve inner subfields (without the four center ones) are $(-0.05 \pm 0.77, 0.03 \pm 0.79)$ mas/yr and between those of the the remaining eight subfields are $(-0.28 \pm 1.67, 0.27 \pm 1.57)$ mas/yr.

3.3 Comparison with other catalogues

An example comparison of our PMs with other catalogues is presented on Fig. 4 and 5 for the case of M55.

Zloczewski et al. (2011) calculated PMs in M55 in four overlapping fields F1–F4. They used images at a resolution of $0.259''/\text{pixel}$. Fig. 4 shows the comparison of PMs for 7822 common stars in M55 from field F1 in their catalogue with those calculated in this work. F1 was chosen because of large number of common stars and long time base (11 years). The two top panels in Fig. 4 are the VPDs of common stars (left – Zloczewski et al. 2011, right – this work). As one could expect given the difference in telescope/camera resolution, the left plot has less spread than the right one. The average difference of PMs for all stars is 0.020 ± 0.013 mas/yr in right ascension and -0.018 ± 0.029 mas/yr in declination. Both values are close to zero, and no systematic trends are visible (see the two bottom panels in Fig. 4). The standard deviation is 1.16 and 2.54 mas/yr, respectively.

Fig. 5 presents the comparison of 480 stars in common with the catalogues of Zloczewski et al. (2011), Sariya et al. (2012), and this work. Sariya et al. (2012) used 26 frames obtained at a resolution of $0.238''/\text{pixel}$. The time span between the two epochs they only used was seven years (five years less than in the present work). The top panels in Fig. 5 are the VPDs of the common stars for Zloczewski et al. (2011, left), Sariya et al. (2012, middle) and this work (right). The middle panel has significantly more spread than the two others. The average PMs difference between Sariya et al. (2012) and this work for all common stars is -0.511 ± 0.160 mas/yr in right ascension and 0.569 ± 0.457 mas/yr in declination, and the standard deviation is 3.510 and 10.012 mas/yr, respectively. The mean values are noticeably different from zero, furthermore the spread around them is large (see the two bottom panels on Fig. 5). A longer time base and a larger number of exposures used for the PM measurements are advantages of our results compared to those of Sariya et al. (2012).

3.4 Completeness

For a given range of magnitudes or angular radial distance from the cluster center (r), the completeness of the measurements was defined as the ratio of the number of stars for which PMs were successfully measured to the number of stars in the master lists in that range. The completeness was measured in intervals of 1 mag in V and 1 arcmin in r . The results for the examples of M4 and 47 Tuc W are shown in Fig. 6. No attempt was made to estimate the completeness of the master lists.

In most GCs the completeness of PM determinations exceeded 70% for $13 < V < 19$ mag, but dropped to $\approx 20\%$ for stars fainter than 20 mag. As a function of r , the completeness first increases (exceeding 70% at $\approx 3'$) but then drops to $\approx 50\%$ or even a few percent in M30 and NGC 362. The minimum at small r is due to the crowding at the centers of the clusters, and the decrease at large r is caused by the fact that for more distant objects fewer epochs are available. In the case of 47 Tuc (Fig. 6b) we observe a steady increase of the completeness with r in both E and W field. This is because the center of the cluster is located at the edge of the reference frame.

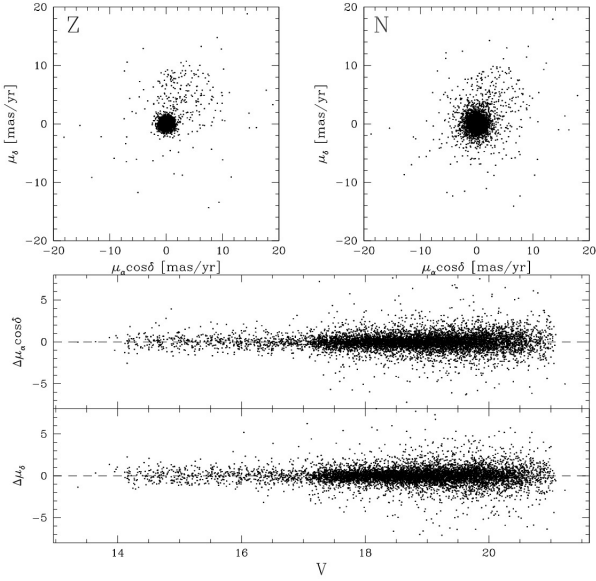


Figure 4. Comparison of PMs of common stars from Zloczewski et al. (2011) (Z) and this work (N) for M55. *Bottom panels:* PM differences in right ascension and declination.

3.5 Cluster membership and membership probability

For the purpose of the text clarity, VPDs for the investigated clusters are shown in the Appendix. They illustrate different degrees of the separation between field and cluster stars. In all cases candidate cluster members concentrate at the coordinate origin. In M4, M22 and NGC 3201 field stars form well defined clumps clearly separate from the cluster stars. In the remaining cases, field and cluster stars overlap partly (e.g. M10) or entirely (e.g. M30). The clump at $(\mu_\alpha \cos \delta, \mu_\delta) = (0.10 \pm 0.01, 7.44 \pm 0.01)$ mas/yr in the VPD of M55 is composed of stars from the Sagittarius dwarf galaxy. Similar clumps in VPDs of NGC 362 at $(\mu_\alpha \cos \delta, \mu_\delta) = (-5.76 \pm 0.01, 1.45 \pm 0.01)$ mas/yr and 47 Tuc at $(\mu_\alpha \cos \delta, \mu_\delta) = (-4.54 \pm 0.02, 1.09 \pm 0.01)$ mas/yr contain members of the SMC.

For each star with a derived PM the *membership status* was obtained and the *membership probability* was calculated. To estimate membership status, we followed the method described by Zloczewski et al. (2011, 2012). Based on the location of a star on the VPD and its PM error (σ_μ) we assigned it to one of the three membership classes; $mem = 0, 1$ or 2 for non-members, probable members and members of the cluster, respectively. To that end, we first divided stars into magnitude bins, each containing 100 stars. For every bin we calculated average values and standard deviations of $\mu_\alpha \cos \delta$ and μ_δ ($M_\alpha, M_\delta, S_\alpha, S_\delta$), and PM errors ($ME_\alpha, ME_\delta, SE_\alpha, SE_\delta$). Next, the parameters $S = (S_\alpha^2 + S_\delta^2)^{1/2}$, $ME = (ME_\alpha^2 + ME_\delta^2)^{1/2}$ and $SE = (SE_\alpha^2 + SE_\delta^2)^{1/2}$ were determined. Stars with $\mu > 3 \cdot S$ were considered non-members ($mem = 0$), stars with $\mu \leq 3 \cdot S$ but $\sigma_\mu > ME + 3 \cdot SE$ were classified as probable cluster members ($mem = 1$), and finally stars with $\mu \leq 3 \cdot S$ and $\sigma_\mu \leq ME + 3 \cdot SE$ were classified

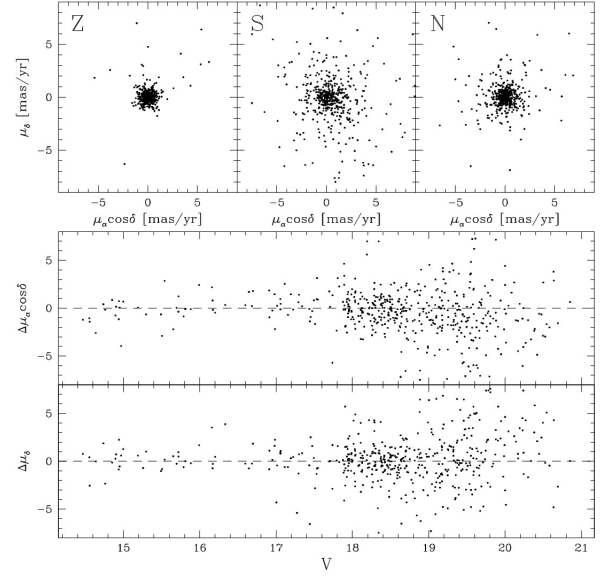


Figure 5. Comparison of PMs of common stars from Zloczewski et al. (2011) (Z), Sariya et al. (2012) (S) and this work (N) for M55. *Bottom panels:* PM differences in right ascension and declination ($S - N$).

Table 4. Statistics of the membership status of stars in the analyzed GCs.

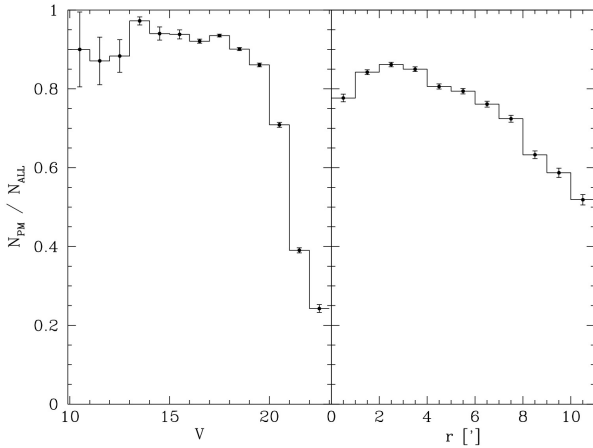
Cluster	$mem = 0$	$mem = 1$	$mem = 2$
M12	3050	435	15635
NGC 6362	4913	302	16636
M4	5870	529	17905
M55	7058	772	31736
M22	45481	1353	40196
NGC 6752	4106	742	32606
NGC 3201	6911	562	25322
M30	1816	312	10510
M10	3138	620	24137
NGC 362	6311	548	17020
M5	6418	992	29632
47 Tuc E	4702	924	36880
47 Tuc W	5623	975	36563

as cluster members ($mem = 2$). Table 4 lists the numbers of stars assigned to each membership class in the analyzed GCs.

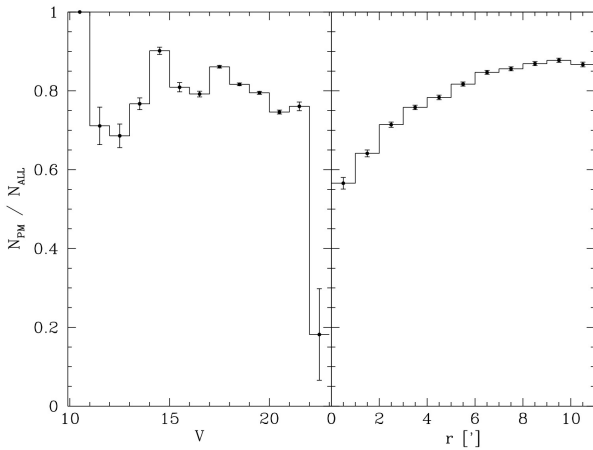
The first attempt to estimate cluster membership probability (P_μ) was undertaken by Vasilevskis et al. (1958), who proposed the formula

$$P = \frac{\Phi_c(\mu_x, \mu_y)}{\Phi_c(\mu_x, \mu_y) + \Phi_f(\mu_x, \mu_y)}, \quad (2)$$

where $\Phi_c(\mu_x, \mu_y)$ and $\Phi_f(\mu_x, \mu_y)$ are bivariate gaussian functions describing VPD distributions of cluster and field stars, respectively. Jones et al. (1988) pointed out that probabilities resulting from Eq. (2) are biased due to two effects. First, parameters in both distributions depend on the brightness of stars. Second, as opposed to the field stars, the spatial distri-



(a) M4



(b) 47 Tuc W

Figure 6. Completeness of our PM catalogue for M4 (a) and 47 Tuc W (b) defined as N_{PM} / N_{ALL} , where N_{PM} – number of stars with PMs and N_{ALL} – number of master list stars in a given interval of V or r . The uncertainties were estimated from the bimodal distribution. The 100% completeness in the 10–11 mag range for 47 Tuc W is misleading, because there is just one star in it.

bution of cluster members is not uniform: their number density decreases with increasing r . Disregarding these two facts leads to underestimation and overestimation of the probabilities for bright and faint stars, respectively. The same holds, respectively, for stars located at the center of the cluster and at its outskirts. Jones et al. (1988) introduced two important modifications. To eliminate the problem of magnitude dependence, they fitted bivariate functions in overlapping magnitude bins. To deal with the second problem, they adopted a model in which the dependence of the surface density of stars on distance from the cluster center was taken into account. A modification of the above method is the *local sample method* described in detail e.g. by Kozhurina-Platais et al. (1995), where for each target star functions Φ_c and Φ_f are fitted to stars from magnitude and distance ranges centered on that star. Another significant modification was introduced by Girard et al. (1989), who proposed to smooth each point on the VPD by replacing it with a normal distribution

with σ equal to the PM error. This way a continuous distribution was obtained, to which the bivariate functions were fitted. In this work, we followed the above methods, slightly modifying them as described below.

First, each i -th star on the VPD was replaced with a two-dimensional normal distribution. Next, a dense grid of (μ_x, μ_y) points was defined on the VPD, and at each grid point the function:

$$f(\mu_x, \mu_y) = \sum_{i=1}^N \sum_{j=1}^N \frac{1}{2\pi\epsilon_{x_i}\epsilon_{y_i}} \exp\left[-\left(\frac{(\mu_x - \mu_{x_i})^2}{2\epsilon_{x_i}^2} + \frac{(\mu_y - \mu_{y_i})^2}{2\epsilon_{y_i}^2}\right)\right] \quad (3)$$

was evaluated, where (μ_{x_i}, μ_{y_i}) are PM components of the i th star, and $(\epsilon_{x_i}, \epsilon_{y_i})$ are PM uncertainties. For all GCs the distance between grid points was 0.1 mas/yr in both coordinates. The smooth distribution thus obtained was then approximated with two two-dimensional distribution functions: a circular Gaussian representing the cluster distribution

$$\Phi_c(\mu_x, \mu_y) = A_1 \cdot \exp\left[-\left(\frac{(\mu_x - \mu_{x01})^2}{2\sigma_x^2} + \frac{(\mu_y - \mu_{y01})^2}{2\sigma_y^2}\right)\right] \quad (4)$$

and an elliptical Gaussian representing field distribution:

$$\Phi_f(\mu_x, \mu_y) = A_2 \cdot \exp\left[-\left(a(\mu_x - \mu_{x02})^2 - b(\mu_x - \mu_{x02})(\mu_y - \mu_{y02}) + c(\mu_y - \mu_{y02})^2\right)\right] \quad (5)$$

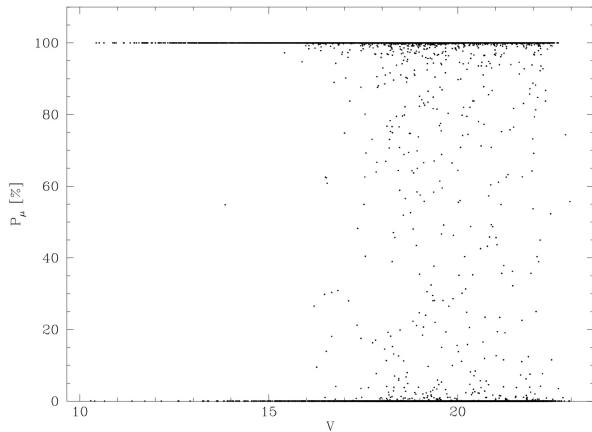
Both functions were fitted in circular apertures centered on (μ_{x01}, μ_{y01}) and (μ_{x02}, μ_{y02}) as a first guess. Depending on the nature of the distribution of stars on the VPD, the apertures used to fit the Gaussians were *separated* (for M4, M22 and NGC 3201) or *concentric* (for the remaining GCs). The aperture radii were multiples of σ defined as an arithmetic mean of σ_x and σ_y . In total, eleven parameters were searched for: $A_1, A_2, \mu_{x01}, \mu_{y01}, \mu_{x02}, \mu_{y02}, \sigma_x, \sigma_y, a, b, c$. PM errors strongly depend on the magnitude of the star. To minimize this effect the fitting was performed in magnitude bins. This approach significantly reduces the computation time in comparison with the local sample method as originally proposed by Kozhurina-Platais et al. (1995). In this study, bins 2 mag wide in V were used, with the upper limit of the first bin located above the horizontal branch, and the lower limit of the last bin at about $V = 23$ mag (depending on the cluster). The bins were overlapping in such a way that the upper limit of the next bin was shifted upwards by 0.025 or 0.05 mag with respect to the lower limit of the previous one (see Table 5). Table 5 summarizes the adopted parameters of apertures and bins.

For each star Φ_c and Φ_f were fitted using the magnitude bin whose center was closest to that star. For the brightest and faintest stars the first and last bins were used, respectively. In principle, the magnitude bins should be subdivided into distance bins, however due to the relatively small angular size of our field of view the spatial distribution was ignored.

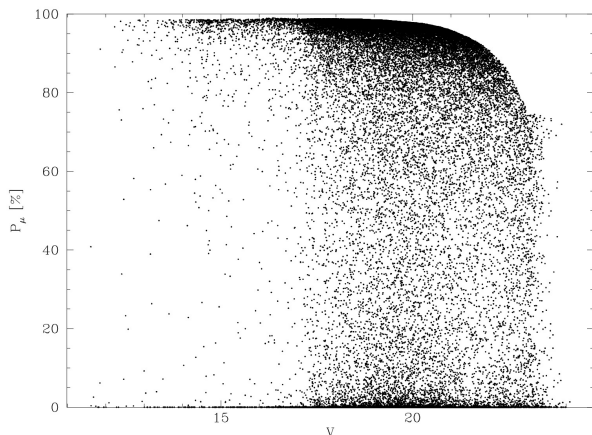
In the end, membership probabilities were calculated using Equation (2) with the improved methods of calculating Φ_c and Φ_f described above. Example results for well (M4) and poorly separated GC (M55) are presented in Fig. 7.

Table 5. Parameters of apertures and bins adopted for Gaussian fitting: c – concentric apertures, s – separated apertures, r_{GC} , r_F – fitting radii for cluster and field, respectively, $MRAN$ – magnitude range in mag, $DBIN$ – shift between magnitude bins in mag.

Cluster	aperture	r_{GC}	r_F	MRAN	DBIN
M12	c	3σ	10σ	13.0 – 23.5	0.025
NGC 6362	c	3σ	10σ	14.5 – 24.0	0.025
M4	s	3σ	8σ	13.0 – 21.2	0.050
M55	c	3σ	15σ	14.0 – 24.0	0.025
M22	s	3σ	8σ	13.0 – 23.5	0.050
NGC 6752	c	3σ	12σ	13.0 – 23.0	0.025
NGC 3201	s	3σ	8σ	13.0 – 24.0	0.025
M30	c	3σ	12σ	14.0 – 23.2	0.025
M10	c	3σ	15σ	13.5 – 23.0	0.025
NGC 362	c	3σ	15σ	14.0 – 23.5	0.025
M5	c	3σ	15σ	13.7 – 23.5	0.025
47 Tuc W	c	3σ	15σ	13.0 – 22.3	0.025
47 Tuc E	c	3σ	15σ	13.0 – 22.3	0.025



(a) M4



(b) M55

Figure 7. Membership probabilities (P_μ) as a function of V magnitude in well separated (M4, see Fig. 7a) and poorly separated GC (M55, see Fig. 7b).

3.6 Comparison of membership probabilities with catalogues of radial velocities

We verified the reliability of the calculated membership probabilities in M4, NGC 3201, M55 and NGC 6752 by comparing the values obtained for individual stars brighter than the MSTO with their radial velocities (v_r) taken from appropriate catalogues. The example result for NGC 6752 is shown in Fig. 8. In this case the analysis was done for 642 red giants, subgiants, horizontal branch stars, and stars from the MSTO vicinity taken from the catalogue of Lardo et al. (2014). Radial velocities of those stars ranged from -88 to 105 km/s. Only stars with velocities close to the mean heliocentric radial velocity (v_h) of NGC 6752 (-26.7 ± 0.2 km/s (Harris 1996)), $v_h \pm 3\sigma_v$ (where $\sigma_v = 4.9$ km/s), are potential cluster members, the remaining ones most probably do not belong to the cluster. Membership probabilities confirm this conclusion. The bottom panel of Fig. 8 shows radial velocities as a function of the membership probability. Stars with high v_r have low probabilities, and most stars with v_r close to v_h have high probabilities. On the top left panel these are marked by red points. The black vertical line indicates CCD saturation level. The middle left panel presents the central part of Fig. A6, with color coded membership probabilities. Stars with high P_μ concentrate around the (0,0) point while stars with low P_μ are located far from this point. On the right panel the same stars are marked on the CMD.

For all four GCs considered in this subsection the overall result of the comparison shows a very good consistency of membership probabilities (as well as membership status) with radial velocities. The majority of stars with v_r close to the v_h of a given cluster have $mem = 2$ and high membership probabilities (from $\overline{P_\mu} > 80\%$ and median value $> 90\%$ for M55 and NGC 6752 to $\overline{P_\mu} = 100\%$ for M4 and NGC 3201, where $\overline{P_\mu}$ is the average membership probability of stars with known v_r). The only exceptions are most probably overexposed stars or stars whose PMs happen to be similar to the PM of the cluster. Stars with v_r far from v_h have $mem = 0$ and $P_\mu < 50\%$.

This experiment allows to define the probability limit $P1$ such that objects with $P \geq P1$ will be considered as cluster members, and those with $P < P1$ as field stars. This limit will be subsequently used to clean the CMDs from interlopers. Keeping in mind that stars used in the above analysis are bright, we chose a value slightly lower than $\overline{P_\mu}$ to make it appropriate also for fainter stars. The average $\overline{P_\mu} - \sigma_{\overline{P_\mu}}$, where $\sigma_{\overline{P_\mu}}$ is a standard deviation, for stars with radial velocities close to v_h from all four clusters, is equal to 69.3%. We adopt a value of $P1 = 70\%$ for all GCs. The consistency of the probability-based cleaning procedure with a given $P1$ can be assessed by determining how many stars with membership class 0 or 1 remain in the cleaned CMD, and how many stars with membership 1 or 2 are removed from the CMD. For the well separated clusters M4, M22 and NGC 3201 the corresponding percentage points are 13.1 and 3.5, while for those poorly separated the values are 3.9 and 33.5, respectively. These cleaning procedures based on both membership status and membership probability are magnitude-dependent, and within each magnitude interval ($V - \Delta V, V + \Delta V$) they reduce to selecting stars from within a circle of a radius r_μ centered on the (0,0) point of the VPD. For status-based cleaning r_μ

increases faster with magnitude than in probability-based cleaning. As a result, the number of faint stars with $mem = 2$ and $P_\mu < 70\%$ can be significantly larger than the number of those with $mem = 0$ and $P_\mu \geq 70\%$. This effect is most pronounced in poorly separated clusters.

4 COLOR-MAGNITUDE DIAGRAMS

Fig. 9–21 present the CMDs of the analyzed cluster fields, and illustrate the effects of CMD cleaning based on membership probabilities. Since the membership status-based cleaning yields very similar results, the corresponding figures are not shown. Left panels include all stars with measured PM and $(B - V)$ color. Middle panels include stars with $P_\mu \geq P1$ and right panels with $P_\mu < P1$, where $P1 = 70\%$. Additionally, in all middle and right panels we marked the positions of known variable stars for which we calculated proper motions. For most GCs, the list of variables was taken from the catalogue of Clement (2001) updated in 2010³. The list of variables for NGC 362 was taken from the recent work of Rozyczka et al. (2016), and for 47 Tuc from Kaluzny et al. (2013a).

Not surprisingly, the CMD-cleaning procedure works best for GCs with VPDs well separated cluster and field stars (see Fig. 11, 13 and 15). In the case of poorly separated GCs some field stars are remaining in the middle panels, and some likely cluster members (in particular, some MS stars) are counted as field objects and assigned to the right panels (see Fig. 9, 12 or 14). For a given cluster, the number of erroneous assignments might be reduced by suitable choice of $P1$, but in general such effects are inevitable while dealing with overlapping populations. The poorest results of CMD cleaning are observed in M5 and 47 Tuc W, where PM uncertainties are particularly large (see Fig. 19 and 21). Moreover, in M5 many RR Lyrae pulsators located in the HB region were assigned to field stars, although most likely they are cluster members measured with large uncertainties because of their location close to the cluster center. For 47 Tuc W more stars were assigned to the field than to the cluster. The variables at the tip of the RGB are overexposed on many images, which again affects their uncertainties. Despite all these problems, the results presented in this Section prove that PMs are quite an efficient means to separate cluster members from field stars.

Membership status-based and membership probability-based cleanings yields similar results. For well separated clusters these are essentially identical but for poorly separated clusters membership probability-based cleaning rejects more stars fainter than $V \approx 19$ mag than the other method. The reason for this was already pointed out in the previous section. Radius r_μ grows faster in the first method than in the second. The limit radius in both methods was not chosen accidentally. Assigning the star with PM less than three times its standard deviation to $mem = 2$ class is very common limit in statistics and in this case should include 99.7% of such stars. The value $P1 = 67\%$ is calculated based on comparison with radial velocities. But both these limits can be changed freely. Additionally, $P1$ can be adopted for

each GC individually or instead of a single value, it might be given as a function, which would describe the $P_\mu(V)$ relation best. We have adopted $P1 = const.$ Membership probability-based cleaning is very sensitive to the number of stars in a given magnitude interval and also to their spatial distribution on VPD (especially the field stars). That does not concern membership status-based cleaning were the average PMs are calculated for equal number of stars in the vicinity of the point (0,0). Despite this, the first of these methods is more stable, because it is based on clear criteria and allows the smooth transition between magnitude intervals. In the second method, the intervals are not overlapping, and this is why the averages and their standard deviations might change significantly while changing the interval limits. Summarizing the above considerations, both cleaning methods have advantages and disadvantages, and neither is unquestionably better than the other.

5 ABSOLUTE PROPER MOTIONS

The derived relative PMs allowed us to estimate the absolute proper motions for six GCs from our sample using close background galaxies (for M55, NGC 362 and 47 Tuc) or distant quasars (for NGC 3201, M10 and M5). The results are presented in Fig. 22 and Table 6 together with absolute PMs from literature.

To determine the relative motion of 47 Tuc and NGC 362 to the SMC we applied the same method as previously used when calculating membership probabilities (see Section 3.5). In the overlapping magnitude ranges we fitted two-dimensional Gaussian functions (given with Eq. 4 and 5) separately to the bulk of the cluster and SMC stars. The aperture radius for the cluster (r_{GC}) and SMC (r_F) were chosen to be 3σ and 1σ , respectively. Next, we calculated the positions of Gaussians centroids, with that of the cluster located at (0,0), as expected.

The PM of a GC relative to a background object is simply the inverse of the PM of the object resulting from the cluster's VPD. We found the PM of 47 Tuc relative to SMC to be $(\mu_\alpha \cos \delta, \mu_\delta) = (4.54 \pm 0.02, -1.09 \pm 0.01)$ mas/yr, where the uncertainties were derived from formal errors of centroid location. This value agrees well with recent estimates by Poleski et al. (2012). Next, we corrected this value by the absolute PM of the SMC based on HST data from Kallivayalil et al. (2013), equal to $(0.772 \pm 0.063, -1.117 \pm 0.061)$ mas/yr and Piatek et al. (2008), equal to $(0.754 \pm 0.061, -1.252 \pm 0.058)$ mas/yr, but also background measurements from Costa et al. (2009), equal to $(1.03 \pm 0.29, -1.09 \pm 0.18)$ mas/yr, Costa et al. (2011), equal to $(0.93 \pm 0.14, -1.25 \pm 0.11)$ mas/yr, Vieira et al. (2010), equal to $(0.98 \pm 0.30, -1.01 \pm 0.29)$ mas/yr, Cioni et al. (2016), equal to $(1.16 \pm 0.07, -0.81 \pm 0.07)$ mas/yr, and recent Tycho-Gaia Astrometric Solution (TGAS) PM from van der Marel & Sahlmann (2016), equal to $(0.874 \pm 0.066, -1.229 \pm 0.047)$ mas/yr. Accounting for the mean absolute PM of the SMC based on above values from literature, we obtained a mean absolute PM of 47 Tuc of $(5.376 \pm 0.032, -2.216 \pm 0.028)$ mas/yr. This result broadly agrees with earlier measurements.

An analogous calculation for NGC 362 gives the relative PM to SMC of $(5.76 \pm 0.01, -1.45 \pm 0.01)$ mas/yr, and a mean absolute PM of $(6.726 \pm 0.032, -2.563 \pm 0.028)$ mas/yr. Addi-

³ <http://www.astro.utoronto.ca/~cclement/read.html>

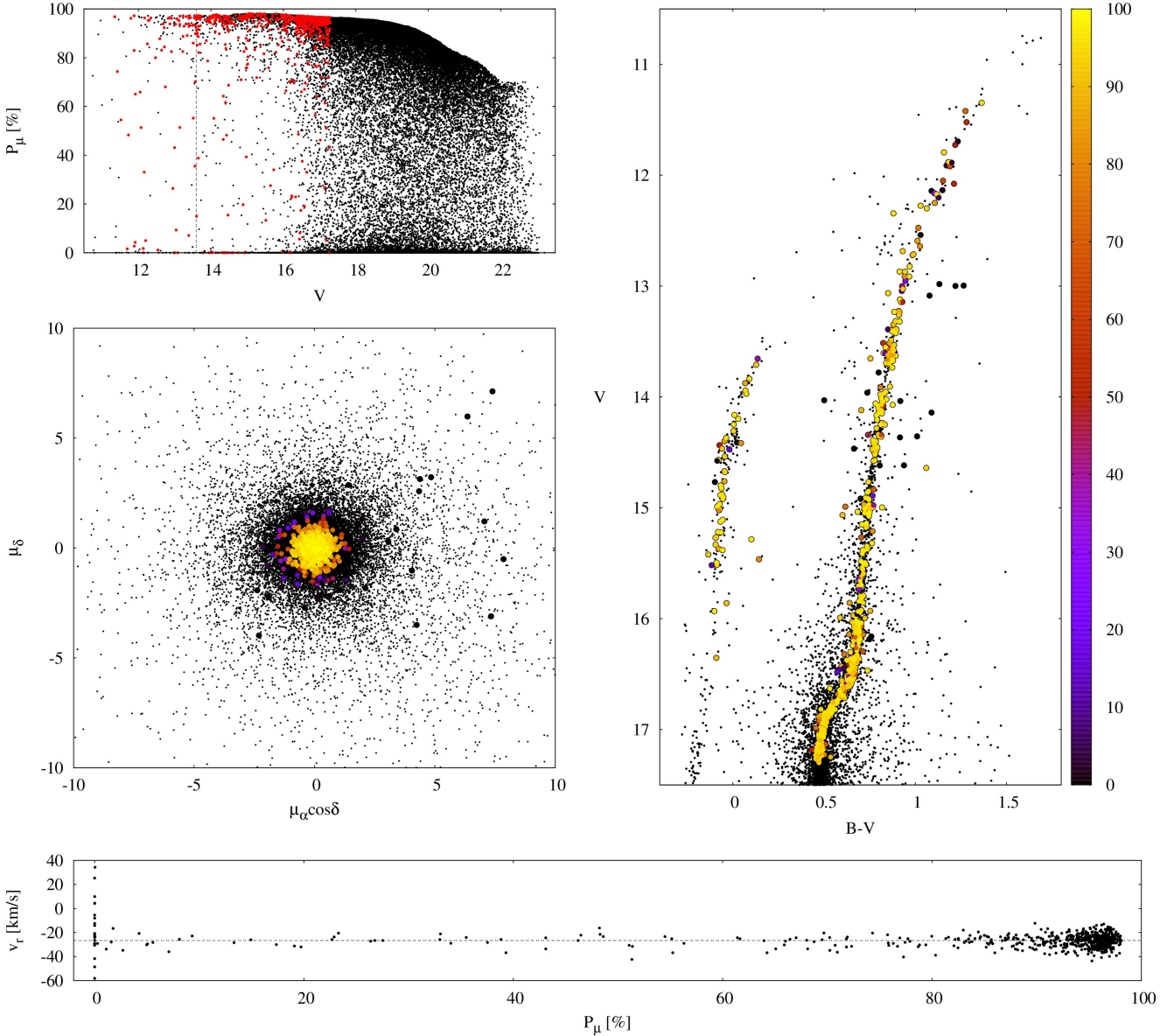


Figure 8. Globular cluster NGC 6752. *Left top:* membership probability (P_μ) as a function of V magnitude. Stars for which radial velocities (v_r) are known are marked with red points. The black vertical line indicates CCD saturation level. *Middle left:* VPD (central part of Fig. A6). Stars with known v_r are marked with larger dots, P_μ is color coded. *Right:* CMD for red giants, subgiants, horizontal branch stars and stars from the MSTO vicinity. *Bottom:* v_r as function of P_μ . Four stars with v_r larger than the axis scale are omitted.

tionally, in the field of NGC 362 we found that the object #2302977 is the quasar candidate J010239.8-705803 from the largest existing quasar catalogue – The Million Quasars catalog⁴ (Milliquas, Flesch 2015). The redshift of this object is unknown but it has an assigned probability of being a quasar of 96%. Based on the PM of this quasar the absolute PM of the cluster is $(7.15 \pm 0.19, -2.21 \pm 0.21)$ mas/yr. These values are equal within the errors, and they coincide with previous estimations, e.g. Odenkirchen et al. (1997).

Since the bulk of the Sagittarius dSph (Sgr-dSph)

galaxy is not well pronounced in the VPD of M55 as the SMC in the above two cases, we decided to use a slightly different approach. We selected stars with $16 < V < 23$ mag lying within 1 mas/yr from the mean motion of the bulk. Stars with PM errors larger than 10 mas/yr were rejected from the sample. In the end, we obtain a sample of 309 stars for which we measured mean motions. The resulting PM of M55 relative to Sgr dSph was estimated to be $(-0.10 \pm 0.01, -7.44 \pm 0.01)$ mas/yr. Following Sohn et al. (2015), we adopted the average PM of the mass center of Sgr dSph to be $(-2.82 \pm 0.11, -1.51 \pm 0.14)$ mas/yr, and the resulting absolute PM of M55 is $(-3.82 \pm 0.11, -8.95 \pm 0.14)$ mas/yr. The latter authors indicate that, because of perspective effects,

⁴ Available on: <http://quasars.org/milliquas.htm>

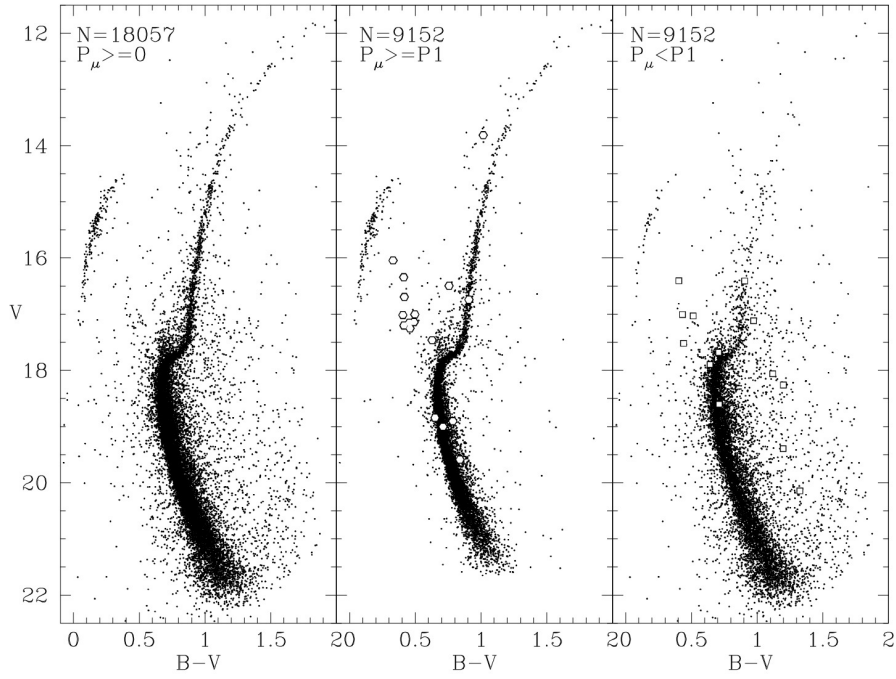


Figure 9. CMD of M12. All stars with PMs and colors measured (*left*); stars with probabilities $P_\mu \geq P_1$ (*middle*); stars with probabilities $P_\mu < P_1$, where $P_1 = 70\%$ (*right*).

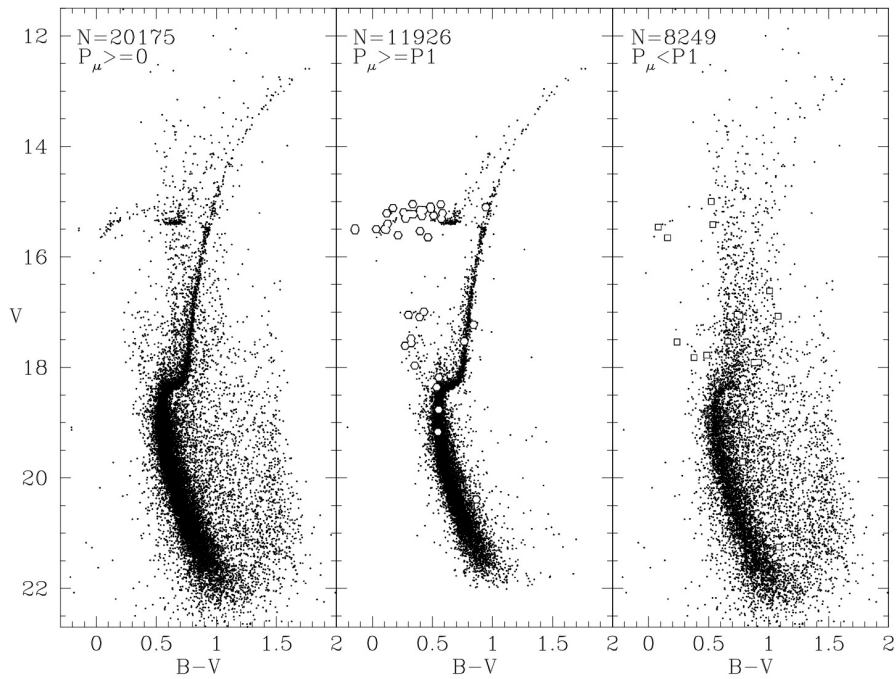


Figure 10. CMD of NGC 6362. All stars with PMs and colors measured (*left*); stars with probabilities $P_\mu \geq P_1$ (*middle*); stars with probabilities $P_\mu < P_1$, where $P_1 = 70\%$ (*right*).

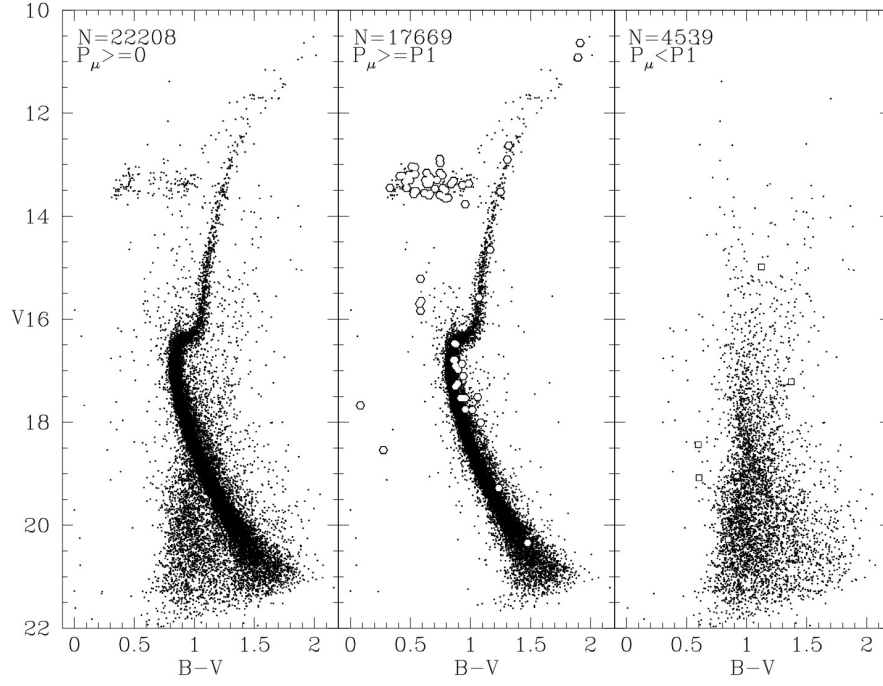


Figure 11. CMD of M4. All stars with PMs and colors measured (*left*); stars with probabilities $P_\mu \geq P1$ (*middle*); stars with probabilities $P_\mu < P1$, where $P1 = 70\%$ (*right*).

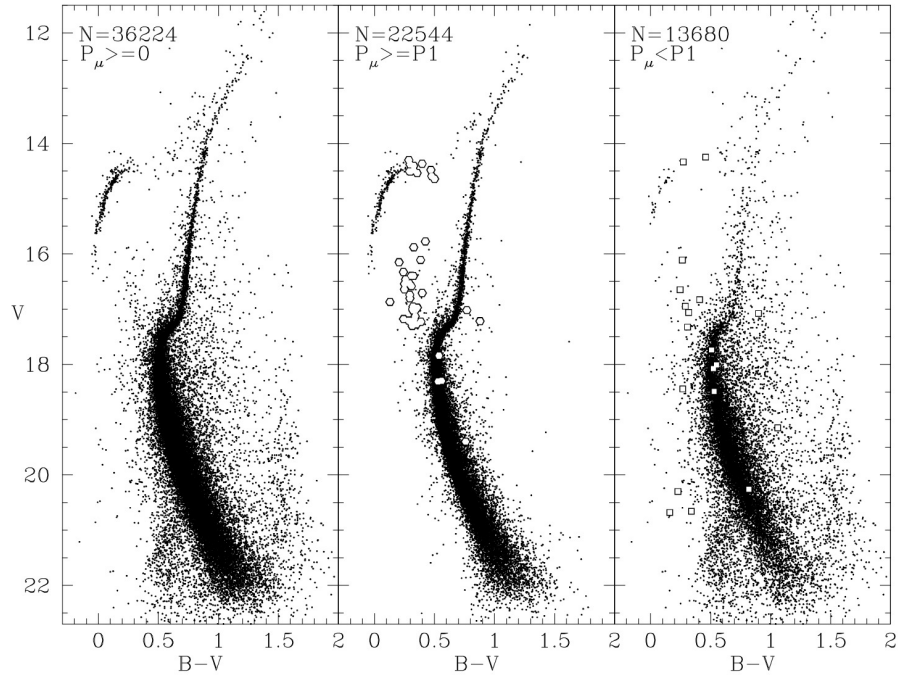


Figure 12. CMD of M55. All stars with PMs and colors measured (*left*); stars with probabilities $P_\mu \geq P1$ (*middle*); stars with probabilities $P_\mu < P1$, where $P1 = 70\%$ (*right*).

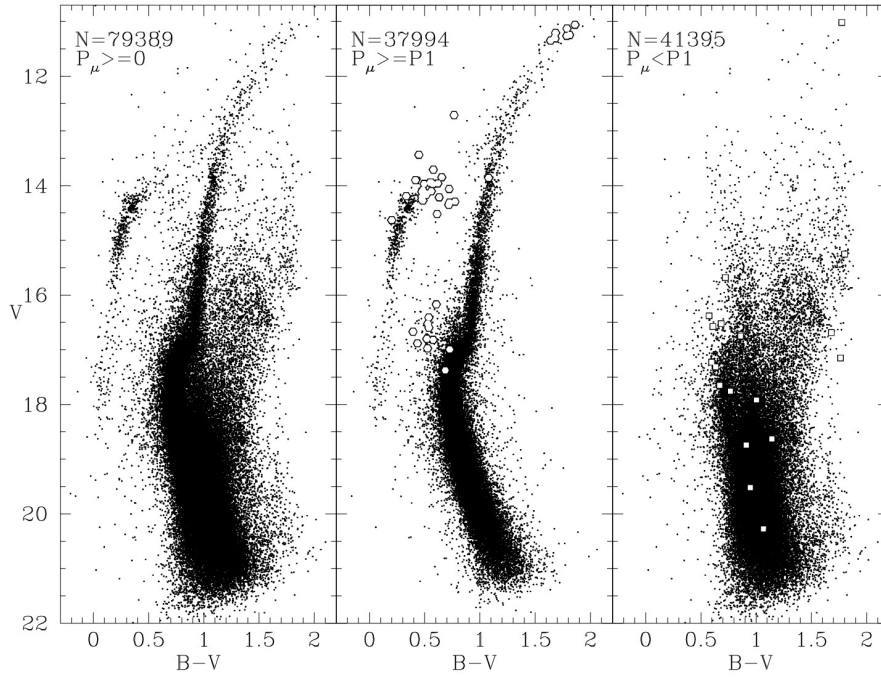


Figure 13. CMD of M22. All stars with PMs and colors measured (*left*); stars with probabilities $P_\mu \geq P1$ (*middle*); stars with probabilities $P_\mu < P1$, where $P1 = 70\%$ (*right*).

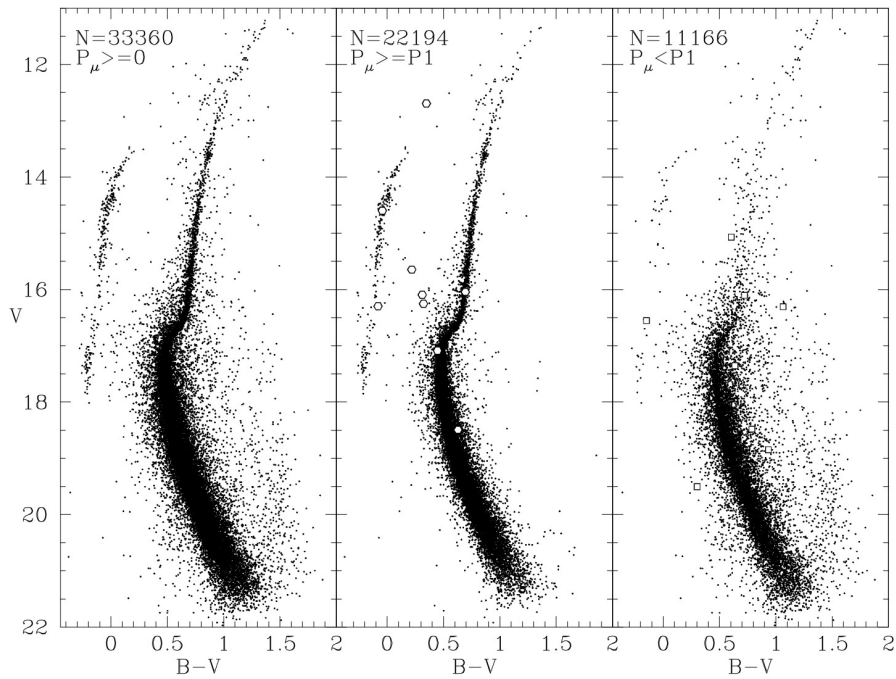


Figure 14. CMD of NGC 6752. All stars with PMs and colors measured (*left*); stars with probabilities $P_\mu \geq P1$ (*middle*); stars with probabilities $P_\mu < P1$, where $P1 = 70\%$ (*right*).

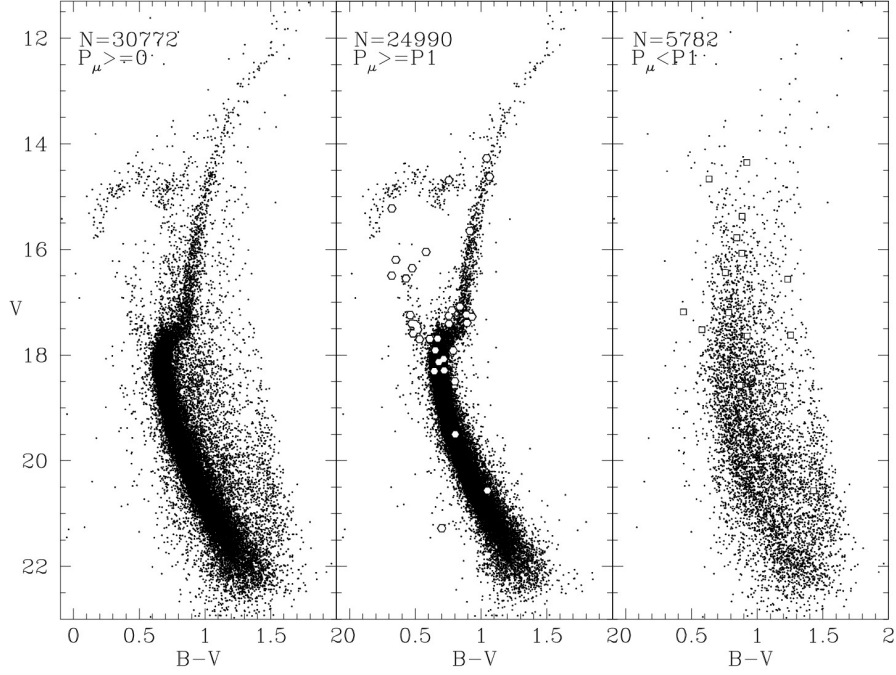


Figure 15. CMD of NGC 3201. All stars with PMs and colors measured (*left*); stars with probabilities $P_\mu \geq P1$ (*middle*); stars with probabilities $P_\mu < P1$, where $P1 = 70\%$ (*right*).

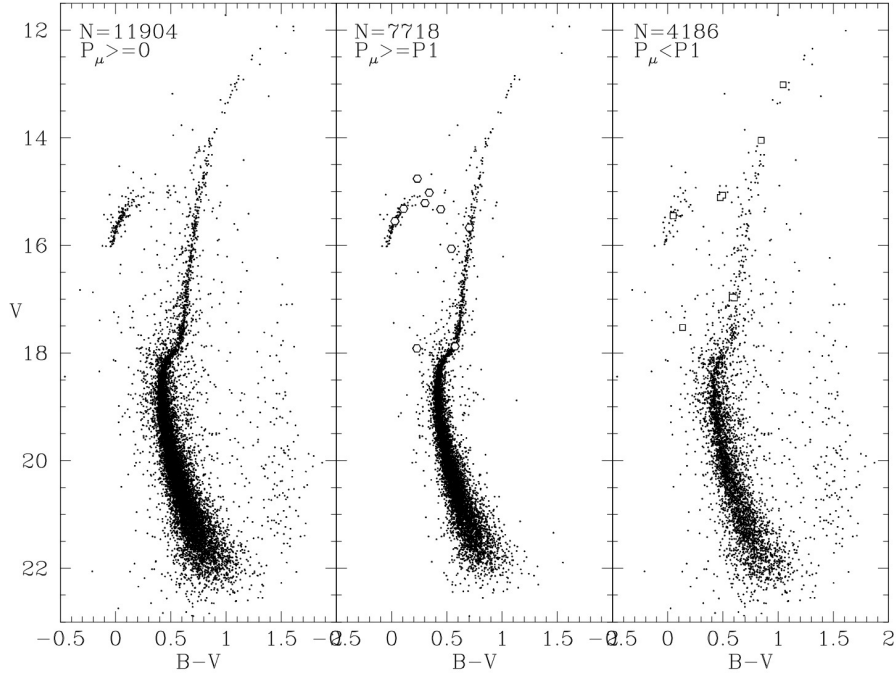


Figure 16. CMD of M30. All stars with PMs and colors measured (*left*); stars with probabilities $P_\mu \geq P1$ (*middle*); stars with probabilities $P_\mu < P1$, where $P1 = 70\%$ (*right*).

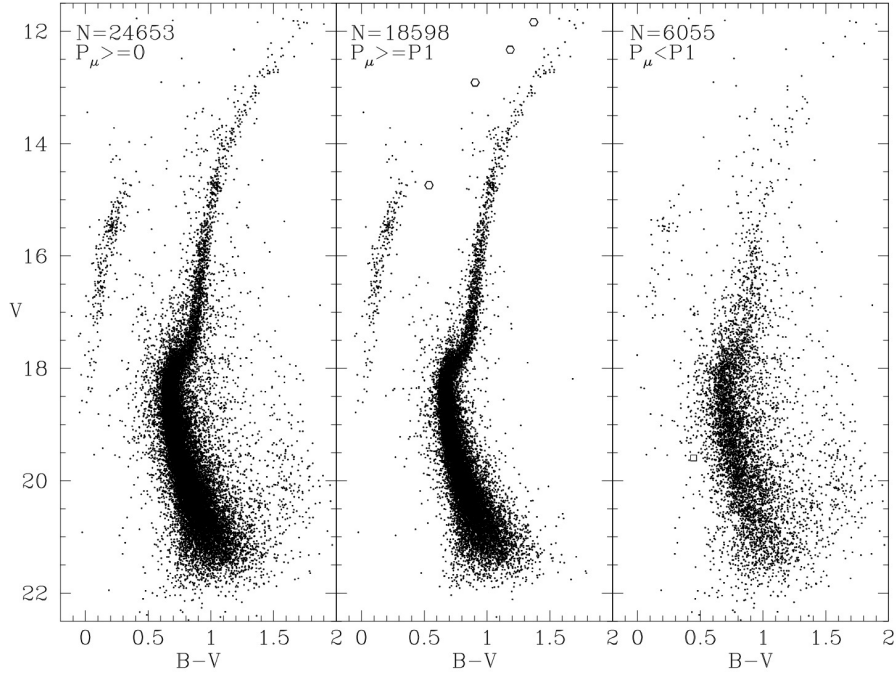


Figure 17. CMD of M10. All stars with PMs and colors measured (*left*); stars with probabilities $P_\mu \geq P1$ (*middle*); stars with probabilities $P_\mu < P1$, where $P1 = 70\%$ (*right*).

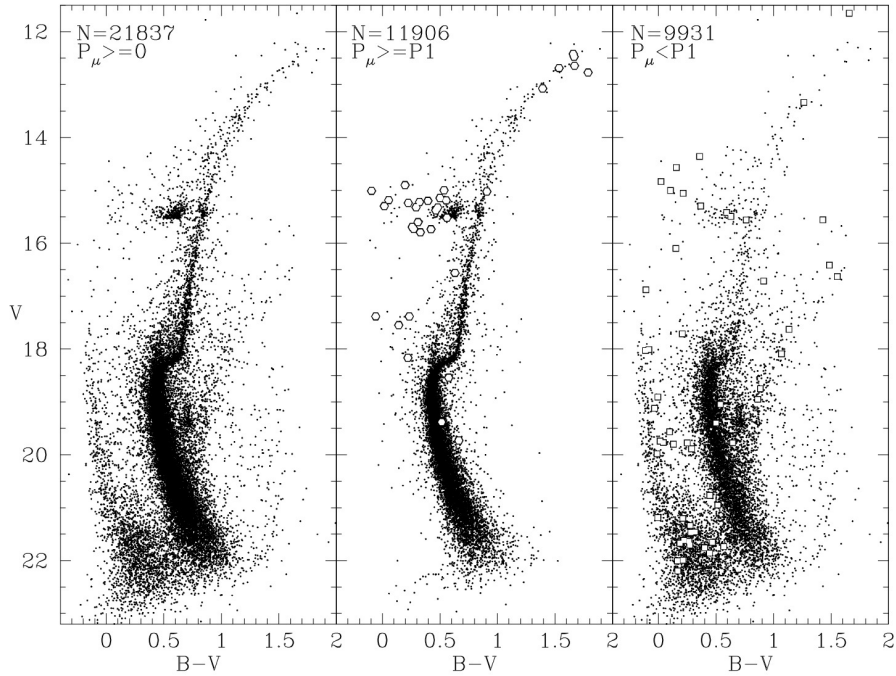


Figure 18. CMD of NGC 362. All stars with PMs and colors measured (*left*); stars with probabilities $P_\mu \geq P1$ (*middle*); stars with probabilities $P_\mu < P1$, where $P1 = 70\%$ (*right*).

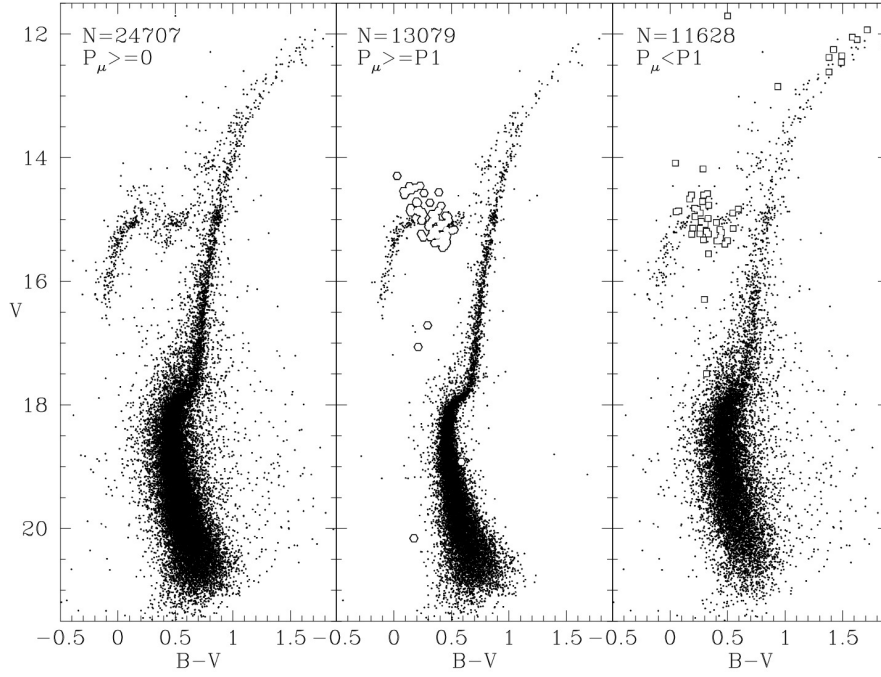


Figure 19. CMD of M5. All stars with PMs and colors measured (*left*); stars with probabilities $P_\mu \geq P1$ (*middle*); stars with probabilities $P_\mu < P1$, where $P1 = 70\%$ (*right*).

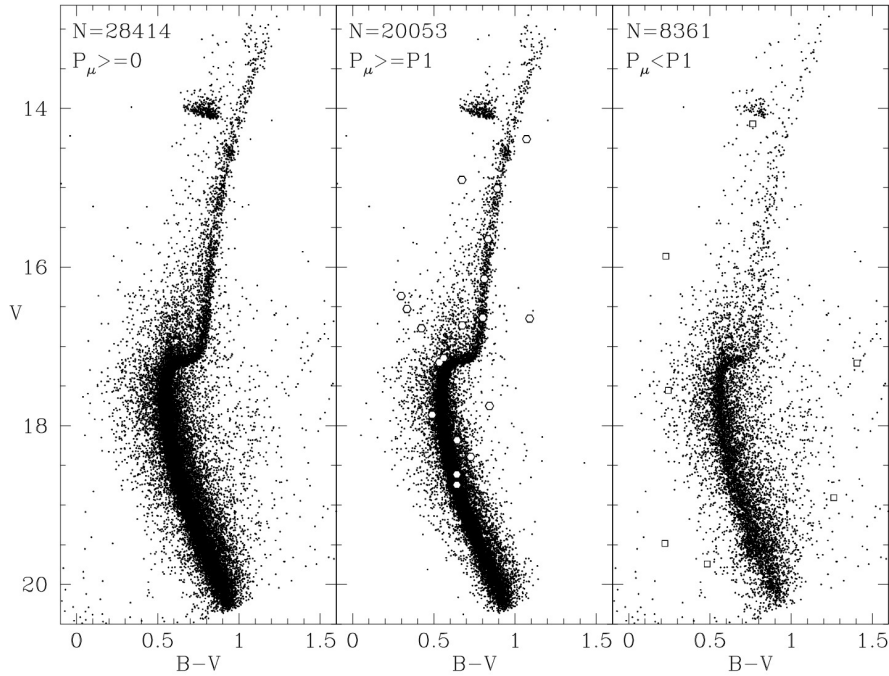


Figure 20. CMD of 47 Tuc field E. All stars with PMs and colors measured (*left*); stars with probabilities $P_\mu \geq P1$ (*middle*); stars with probabilities $P_\mu < P1$, where $P1 = 70\%$ (*right*).

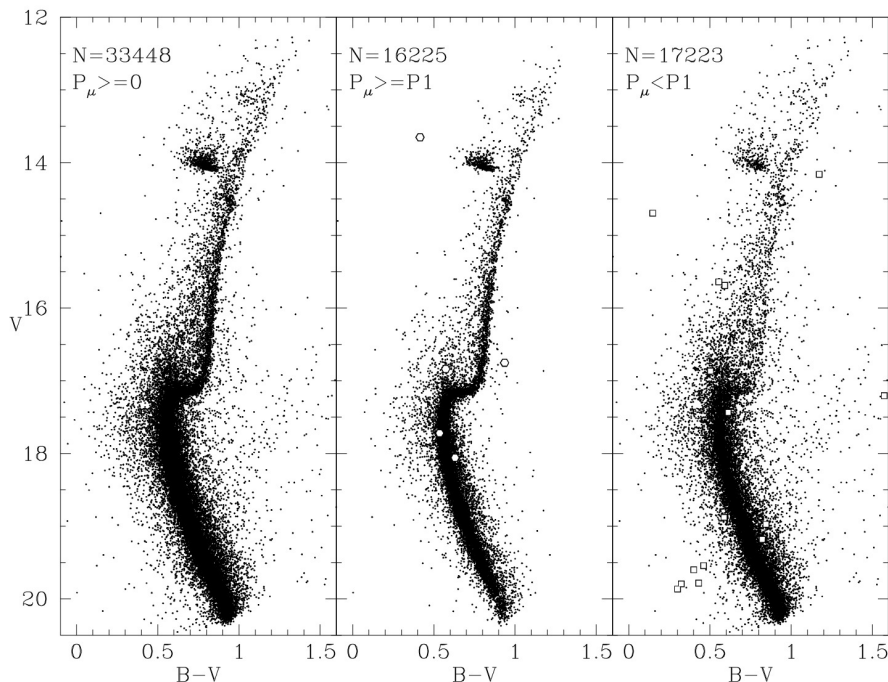


Figure 21. CMD of 47 Tuc field W. All stars with PMs and colors measured (*left*); stars with probabilities $P_\mu \geq P1$ (*middle*); stars with probabilities $P_\mu < P1$, where $P1 = 70\%$ (*right*).

measuring PMs in different parts of the extremely stretched Sgr dSph gives different results. This might be the reason why our value differs from $(-3.31 \pm 0.10, -9.14 \pm 0.15)$ mas/yr obtained by [Zloczewski et al. \(2011\)](#) for the absolute PM of M55.

We identified objects #260440 and #260472 in the field of M10 to be the quasars SDSS J165714.34-041625.9 and SDSS J165713.57-041620.7 from the Milliquas catalogue. Their redshifts are $z \approx 1.4$ and 2.5 , respectively. In the catalogue they have assigned probability of being a quasar equal to 95% and 96%. The weighted mean motion of these objects results in an absolute PM of M10 of $(-4.82 \pm 0.15, -6.18 \pm 0.13)$ mas/yr. This value coincides within the errors with the estimate given by [Chen et al. \(2000\)](#).

In the field of M5 we found six Milliquas objects. We identified object #2600420 as J151840.4+015352, #4500589 as J151819.4+015918, #4401792 as J151819.1+020152, #4201481 as SDSS J151810.74+021257.2, #1600139 as SDSS J151857.62+015345.9 and #3100796 as SDSS J151824.02+021347.6. For the first three objects there is no redshift given in the catalogue, and the assigned probabilities of being a quasar are 83%, 80% and 86%, respectively. Redshifts of the remaining objects are equal to 2.8, 1.0 and 1.2, respectively, and the assigned probabilities range from 98% to 99%. The absolute PM of M5 based on the weighted mean of motions of all six quasars is $(1.22 \pm 0.09, -5.40 \pm 0.08)$ mas/yr. We found that the object SDSS J151810.74+021257.2 in the USNO catalogue is identified with object 0922-0339533 which has significant absolute PM, so most probably it is a misidentification. The absolute PM of M5 based only on the two quasars for which the redshifts are known is $(2.63 \pm 0.34, -10.75 \pm 0.34)$ mas/yr.

The discrepancy between both values comes from the fact that only two quasars with known redshifts have significant PMs (#1600139 and #3100796), the remaining four have PMs close to zero.

The object #337214 in the field of NGC 3201 in [Kaluzny et al. \(2016\)](#) was found to be a quasar with a redshift $z \approx 0.5$ and is an X-ray counterpart ([Moth et al. 2016](#), , object J101715.62-462253.2). It does not appear in the Milliquas catalogue. Based on its relative PM, the absolute PM of NGC 3201 is $(8.52 \pm 1.17, -5.92 \pm 1.11)$ mas/yr. The absolute PM of NGC 3201 was measured by [Zloczewski et al. \(2012\)](#) with a result of $(9.11 \pm 0.47, -3.94 \pm 0.54)$ mas/yr. The difference between these two result is statistically insignificant, but both of these estimates are significantly different from values presented by [Casetti-Dinescu et al. \(2007\)](#) or [Dambis \(2006\)](#).

In most cases, our absolute PMs agree within the errors with the previous estimations. Quasars provide the best and most straightforward means to determine the absolute PMs of GCs. Unfortunately, only very few of them have been found so far in cluster fields, especially in southern hemisphere, where optical quasar catalogues are far from being complete.

6 SUMMARY

Based on data collected between 1997 to 2015 we obtained proper motions of over 446 000 stars in the fields of twelve nearby Galactic globular clusters: M12, NGC 6362, M4, M55, M22, NGC 6752, NGC 3201, M30, M10, NGC 362, M5, and 47 Tuc. The measurements were made using procedures similar to those used by [Anderson et al. \(2006\)](#) and

[p]

Table 6. Absolute PMs for six GCs.

ID	This work		Literature		Reference
	$\mu_{\alpha} \cos \delta$ [mas/yr]	μ_{δ} [mas/yr]	$\mu_{\alpha} \cos \delta$ [mas/yr]	μ_{δ} [mas/yr]	
M55	-3.82 ± 0.11	-8.95 ± 0.14	-1.42 ± 0.62	-10.25 ± 0.64	Dinescu et al. (1999)
NGC 3201	8.52 ± 1.17	-5.92 ± 1.11	-1.33 ± 0.42	-7.86 ± 0.40	Dambis (2006)
			-3.31 ± 0.10	-9.14 ± 0.15	Zloczewski et al. (2011)
			0.17 ± 0.83	-1.06 ± 0.60	Dambis (2006)
M10	-4.82 ± 0.15	-6.18 ± 0.13	5.28 ± 0.32	-0.98 ± 0.33	Casetti–Dinescu et al. (2007)
			-6.00 ± 1.00	-3.30 ± 1.00	Odenkirchen et al. (1997)
NGC 362	6.726 ± 0.032	-2.563 ± 0.028 ¹	-5.50 ± 1.20	-6.20 ± 1.20	Chen et al. (2000)
			-4.81 ± 0.72	-0.01 ± 0.90	Dambis (2006)
			4.43 ± 1.02	-3.99 ± 1.04	Tucholke (1992b)
M5	7.15 ± 0.19	-2.21 ± 0.21 ²	5.70 ± 1.00	-1.10 ± 1.00	Odenkirchen et al. (1997)
			10.20 ± 0.59	-7.19 ± 0.57	Dambis (2006)
47 Tuc	5.376 ± 0.032	-2.216 ± 0.028	5.20 ± 1.70	-14.20 ± 1.30	Cudworth & Hanson (1993)
			6.70 ± 0.50	-7.80 ± 0.40	Scholz et al. (1996)
			3.30 ± 1.00	-10.10 ± 1.00	Odenkirchen et al. (1997)
47 Tuc	5.376 ± 0.032	-2.216 ± 0.028	-3.60 ± 0.74	-9.54 ± 0.73	Dambis (2006)
			6.43 ± 2.10	-2.99 ± 2.11	Tucholke (1992a)
			3.40 ± 1.70	-1.90 ± 1.50	Cudworth & Hanson (1993)
			7.00 ± 1.00	-5.30 ± 1.00	Odenkirchen et al. (1997)
			6.60 ± 1.90	-3.40 ± 0.60	Freire et al. (2001)
			5.30 ± 0.60	-3.30 ± 0.60	Freire et al. (2003)
			4.716 ± 0.035	-1.325 ± 0.021	Anderson et al. (2003)
			6.73 ± 0.30	-1.54 ± 0.29	Dambis (2006)
			6.90 ± 1.00	-2.1 ± 1.00	Girard et al. (2011) ^a
			4.41 ± 0.67	-1.12 ± 0.55	Poleski et al. (2012) ^a
47 Tuc	5.376 ± 0.032	-2.216 ± 0.028	7.26 ± 0.03	-1.25 ± 0.03	Cioni et al. (2016)
			5.50 ± 0.70	-3.99 ± 0.55	Watkins et al. (2016)

¹ PM relative to SMC and corrected for its absolute PM. ² PM based on single quasar.

³ PM based on two quasars. ⁴ PM based on six quasars.

^a PM relative to SMC.

Zloczewski et al. (2011, 2012). Each of those stars was assigned to one of the three membership classes, and its membership probability was calculated. Both approaches allow to efficiently separate field stars from cluster members on CMDs. For six GCs the absolute PMs were obtained. The catalogues of the derived PMs will be freely accessible from <http://case.camk.edu.pl/> and Vizier/CDS.

ACKNOWLEDGEMENTS

WN, JK, MR and WP were partly supported by the grant DEC-2012/05/B/ST9/03931 from the Polish National Science Center.

REFERENCES

Anderson J., King I. R., 2003, *AJ*, 126, 772
 Anderson J., Bedin L. R., Piotto G., Yadav R. S., Bellini A., 2006, *A&A*, 454, 1029
 Anderson J., van der Marel R. P., 2010, *ApJ*, 710, 1032
 Bellini A., Piotto G., Bedin L. R., Anderson J., Platais I., Momany Y., Moretti A., Milone A. P., Ortolani S., 2009, *A&A*, 493, 959
 Bellini A., Anderson J., van der Marel R. P., Watkins L. L., King I. R., Bianchini P., Chaname J., Chandar R., Cool A. M., Ferraro F. R., Ford H., Massari D., 2014, *AJ*, 797, 115
 Casetti-Dinescu D. I., Girard T. M., Herrera D., van Altena W. F., López C. E., Castillo D. J., 2007, *AJ*, 134, 195

Cioni M. L.; Bekki K., Girardi L., de Grijs R., Irwin M. J., Ivanov V. D., Marconi M., Oliveira J. M., Piatti A. E., Ripepi V., van Loon J. Th., 2016, *A&A*, 586, 16
 Chen L., Geffert M., Wang J. J., Reif K., Braun J. M., 2000, *A&AS*, 145, 223
 Clement C. M., 2001, *AJ*, 122, 2587
 Costa E., Méndez R. A., Pedreros M. H., Moyano M., Gallart C., Noël N., Baume G., Carraro G., 2009, *AJ*, 137, 4339
 Costa E., Méndez R. A., Pedreros M. H., Moyano M., Gallart C., Noël N., 2011, *AJ*, 141, 136
 Cudworth K. M., 1980, *IAUS*, 85, 431
 Cudworth K. M., Hanson R. B., 1993, *AJ*, 105, 168
 Dambis A. K., 2006, *Astronomical and Astrophysical Transactions*, 25, 185
 Dinescu D. I., Girard T. M., van Altena W. F., 1999, *AJ*, 117, 1792
 Drukier G. A., Baily C. D., Van Altena W. F., Girard T. M., 2003, *AJ*, 125, 2559
 Ebbighausen E. G., 1942, *AJ*, 50, 1
 Flesch E. W., 2015, *PASA*, 32, 10
 Freire P. C., Camilo F., Lorimer D. R., Lyne A. G., Manchester R. N., D’Amico N., 2001, *MNRAS*, 326, 901
 Freire P. C., Camilo F., Kramer M., Lorimer D. R., Lyne A. G., Manchester R. N., D’Amico N., 2003, *MNRAS*, 340, 1359
 Girard T. M., Grundy W. M., Lopez C. E., van Altena W. F., 1989, *AJ*, 98, 227
 Girard T. M. et al., 2011, *AJ*, 142, 15
 Harris W. E., 1996, *AJ*, 112, 1487
 Jones B. F., Walker M. F., 1988, *AJ*, 95, 1755
 Kallivayalil N., van der Maerl R. P., Besla G., Anderson J., Alcock C., 2013, *ApJ*, 764, 161

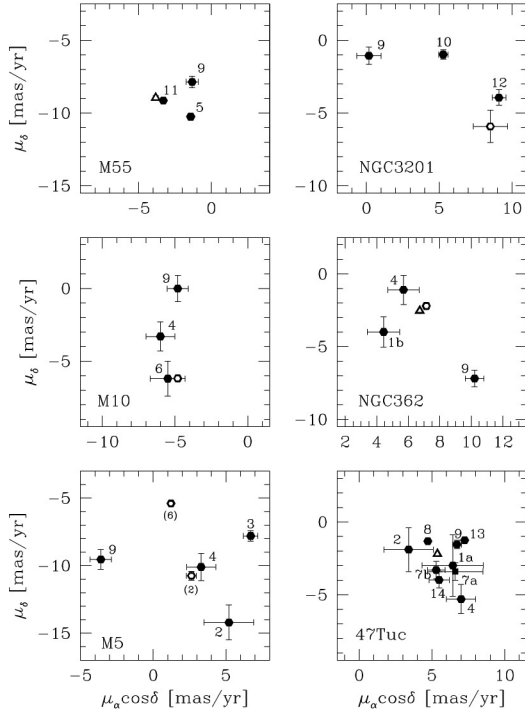


Figure 22. Absolute PMs for six GCs. Black and white triangles mark absolute PMs from this work calculated relative to nearby galaxy and then corrected for its absolute PM from the literature. Black and white points mark absolute PMs calculated basing on quasars identified in the field of a given GC, where (6), (3) – absolute PM calculated basing on six and three quasars, respectively. Black points mark absolute PMs from the literature, where 1*a*, *b* – Tucholke (1992*a*,*b*), 2 – Cudworth & Hanson (1993), 3 – Scholz et al. (1996), 4 – Odenkirchen et al. (1997), 5 – Dinescu et al. (1999), 6 – Chen et al. (2000), 7*a*, *b* – Freire et al. (2001, 2003), 8 – Anderson et al. (2003), 9 – Dambis (2006), 10 – Casetti–Dinescu et al. (2007), 11 – Zloczewski et al. (2011), 12 – Zloczewski et al. (2012), 13 – Cioni et al. (2016), 14 – Watkins et al. (2016).

Kaluzny J., Thompson I. B., Krzeminski W., Preston G. W., Pych W., Rucinski S. M., Schwarzenberg-Czerny A., Scheetman S. A., Stachowski G., in American Institute of Physics Conference Series, 752, Stellar Astrophysics with the World's Largest Telescopes, Mikolajewska J., Olech A., eds., 70
 Kaluzny J., Rozyczka M., Pych W., Krzeminski W., Zloczewski K., Narloch W., Thompson I. B., 2013*a*, *AcA*, 63, 309
 Kaluzny J., Thompson I. B., Dotter A., Rozyczka M., Schwarzenberg-Czerny A., Burley G., Mazur B., Rucinski S. M., 2015*a*, *AJ*, 150, 155
 Kaluzny J., Thompson I. B., Narloch W., Pych W., Rozyczka M., 2015*b*, *AcA*, 65, 267
 Kaluzny J., Rozyczka M., Thompson I. B., Narloch W., Mazur B., Pych W., Schwarzenberg-Czerny A., 2016, *AcA*, 66, 31
 Kozhurina-Platais V., Girard T. M., Platais I., van Altena W. F., Ianna P. A., Cannon R. D., 1995, *AJ*, 109, 672
 Kuijken K., Rich R. M., 2002, *AJ*, 124, 2054
 Landolt A. U., 1992, *AJ*, 104, 340
 Lardo C. et al., 2014, *VizieR Online Data Catalog*, 357
 Lindegren L. et al., 2016, *ArXiv e-prints*
 Mazur B., Krzeminski W., Thompson I. B., 2003, *MNRAS*, 340, 1205

McLaughlin D. E., Anderson J., Meylan G., Gebhardt K., Pryor C., Minniti D., Phinney S., 2006, *ApJS*, 166, 249
 Mignard F., 2005, *ASPC*, 338, 15
 Motch C. et al., 2016, eprint arXiv:1609.00809
 Odenkirchen M., Brosche P., Geffert M., Tucholke H. J., 1997, *NewA*, 2, 477
 Pancino E., Bellazzini M., Marinoni S., *MmSAI*, 84, 83
 Pancino E., Bellazzini M., Giuffrida G., Marinoni S., eprint arXiv:1701.03003
 Piatek S., Pryor C., Olszewski E. W., 2008, *AJ*, 135, 1024
 Poleski R., Soszyński I., Udalski A., Szymański M. K., Kubiak M., Pietrzyński G., Wyrzykowski L., Ulaczyk K., 2012, *AcA*, 62, 1
 Rozyczka M., Thompson I. B., Narloch W., Pych W., Schwarzenberg-Czerny A., 2016, *AcA*, 66, 307
 Sariya D. P., Yadav R. K. S., Bellini A., 2012, *A&A*, 543, A87
 Scholz R. D., Odenkirchen M., Hirte S., Irwin M. J., Borngen F., Ziener R., 1996, *MNRAS*, 278, 251
 Simunovic M., Puzia T. H., 2016, *MNRAS*, 462, 3401
 Smolec R., Moskalik P., Kałuzny J., Pych W., Różyczka M., Thompson I. B., 2017, *MNRAS*, 159
 Sohn S. T., van der Marel R. P., Carlin J. L., Majewski S. R., Kallivayalil N., Law D. R., Anderson J., Siegel M. H., 2015, *ApJ*, 803, 56
 Stetson P. B., 1987, *PASP*, 99, 191
 Stetson P. B., 1990, *PASP*, 102, 932
 Thompson I. B., Kaluzny J., Rucinski S. M., Krzeminski W., Pych W., Dotter A., Burley G. S., 2010, *AJ*, 139, 329
 Tucholke H. J., 1992*a*, *A&AS*, 93, 311
 Tucholke H. J., 1992*b*, *A&AS*, 93, 293
 van der Marel R. P., Sahlmann J., 2016, *ApJL*, 832, 23
 Vasilevskis S., Klemola A., Preston G., 1958, *AJ*, 63, 387
 Vieira, K., Girard T. M., van Altena W. F., Zacharias N., Casetti–Dinescu D. I., Korchagin V. I., Platais I., Monet D. G., López C. E., Herrera D., Castillo D. J., 2010, *AJ*, 140, 1934
 Watkins L. L., van der Marel R. P., Bellini A., Anderson J., 2015, *AJ*, 803, 29
 Watkins L. L., van der Marel R. P., 2016, eprint arXiv:1611.03170
 Wozniak P. R., 2000, *AcA*, 50, 421
 Zacharias N., Finch C. T., Girard T. M., Henden A., Bartlett J. L., Monet D. G., Zacharias M. I., 2012, *VizieR Online Data Catalog*, 1322
 Zloczewski K., Kaluzny J., Thompson I. B., 2011, *MNRAS*, 414, 3711
 Zloczewski K., Kaluzny J., Rozyczka M., Krzeminski W., Mazur B., 2012, *AcA*, 62, 357

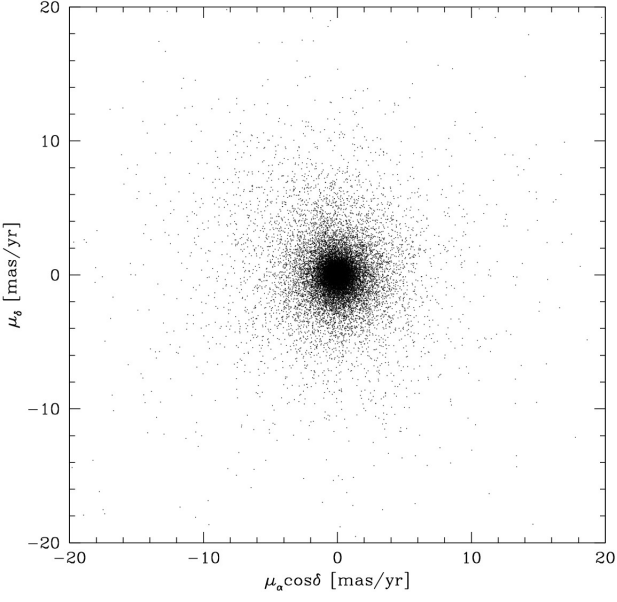


Figure A1. Vector point diagram (VPD) for M12.

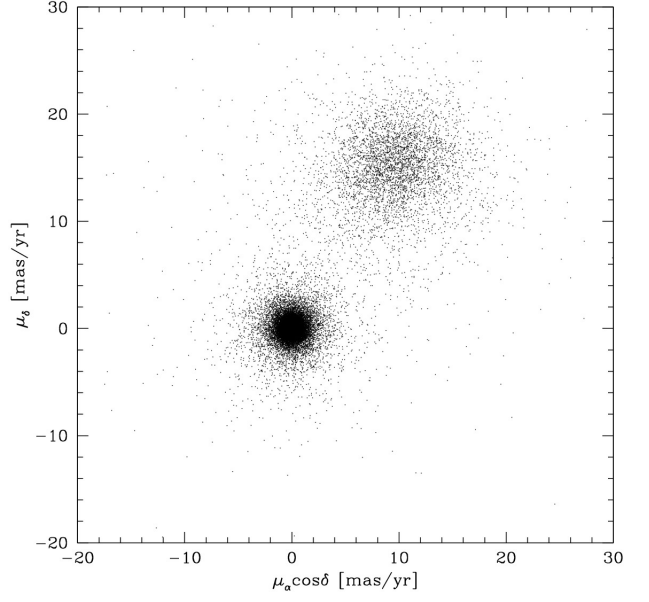


Figure A3. VPD for M4.

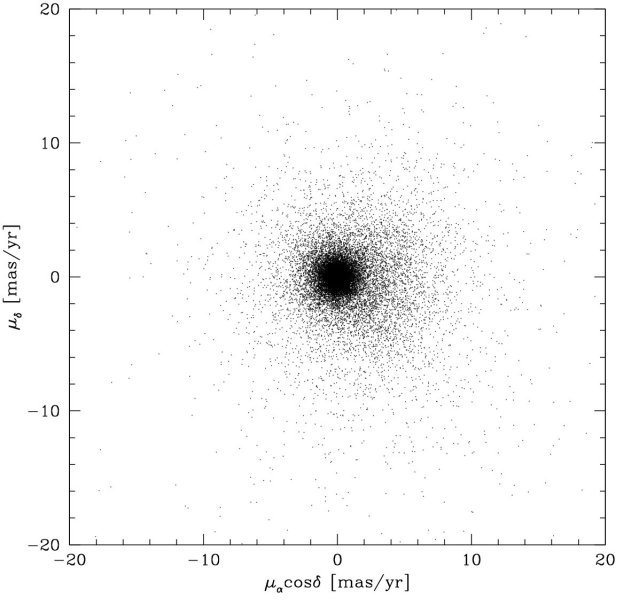


Figure A2. VPD for NGC 6362.

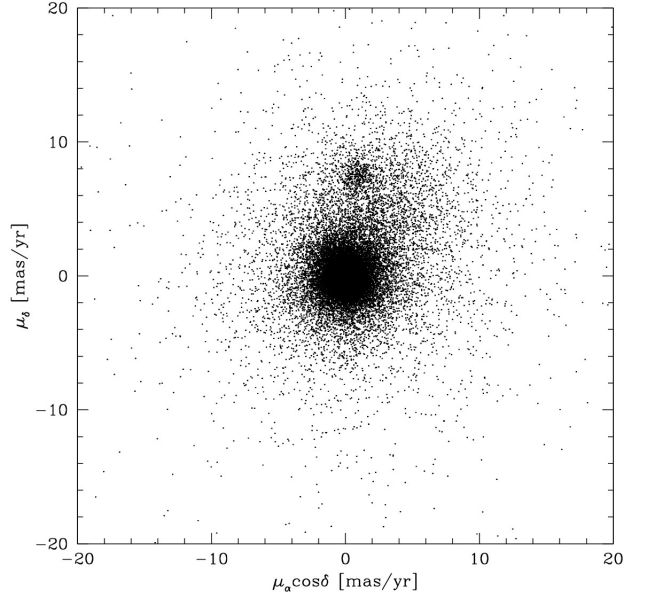


Figure A4. VPD for M55.

APPENDIX A: SOME EXTRA MATERIAL

Fig. A1–A13 present VPDs for all GCs in this study.

This paper has been typeset from a $\text{\TeX}/\text{\LaTeX}$ file prepared by the author.

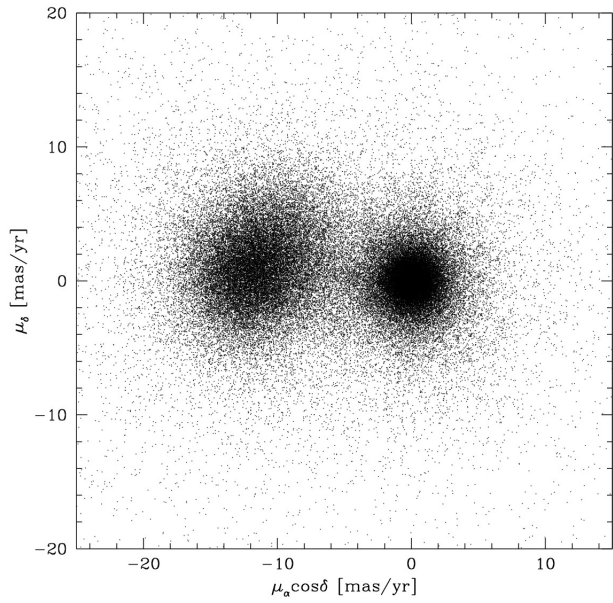


Figure A5. VPD for M22.

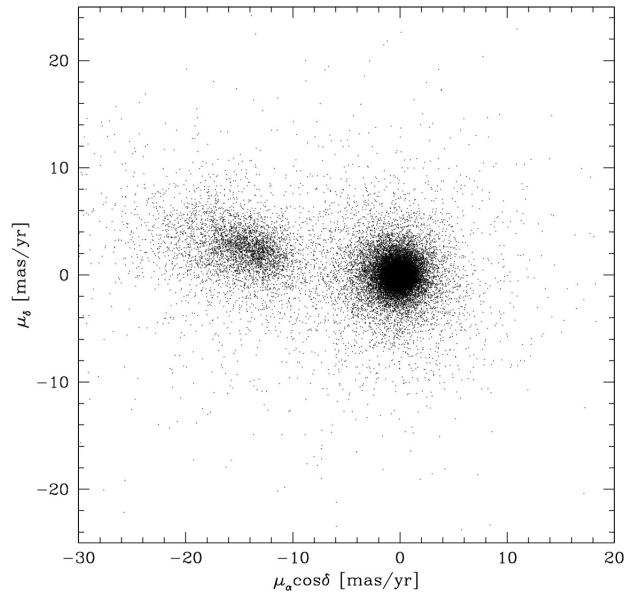


Figure A7. VPD for NGC 3201.

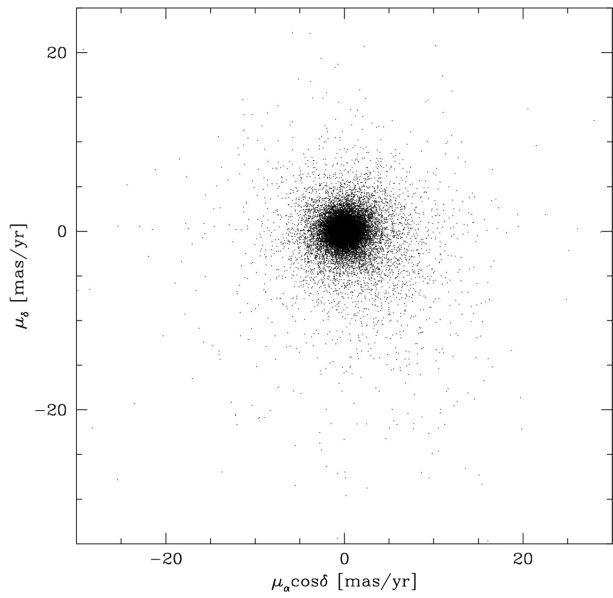


Figure A6. VPD for NGC 6752.

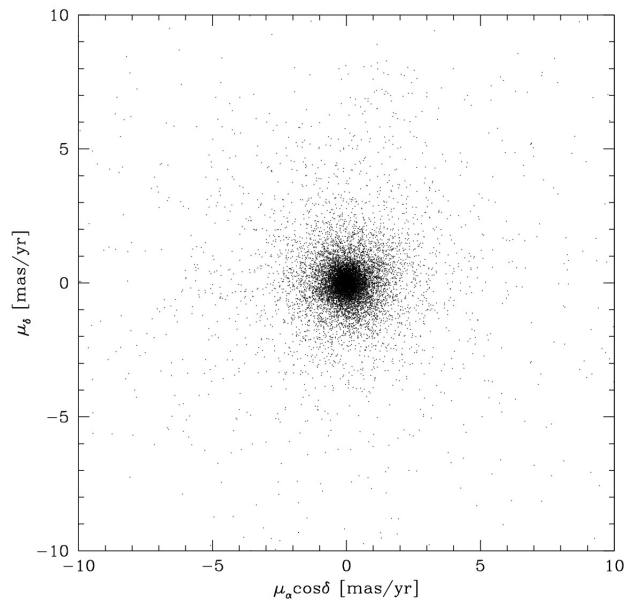


Figure A8. VPD for M30.

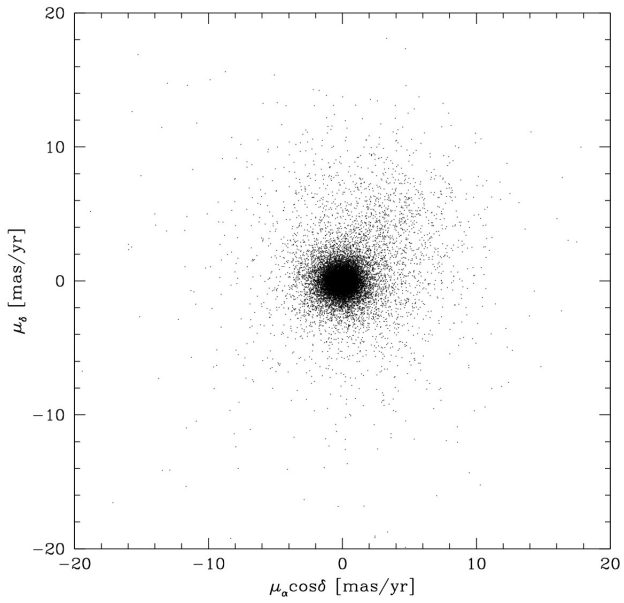


Figure A9. VPD for M10.

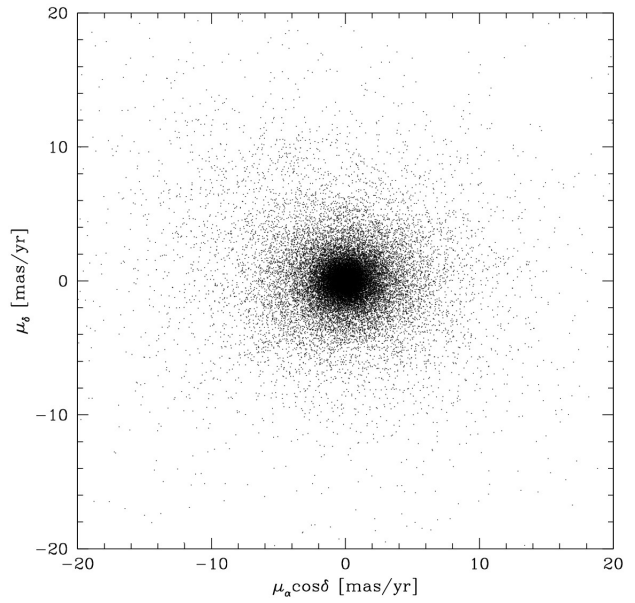


Figure A11. VPD for M5.

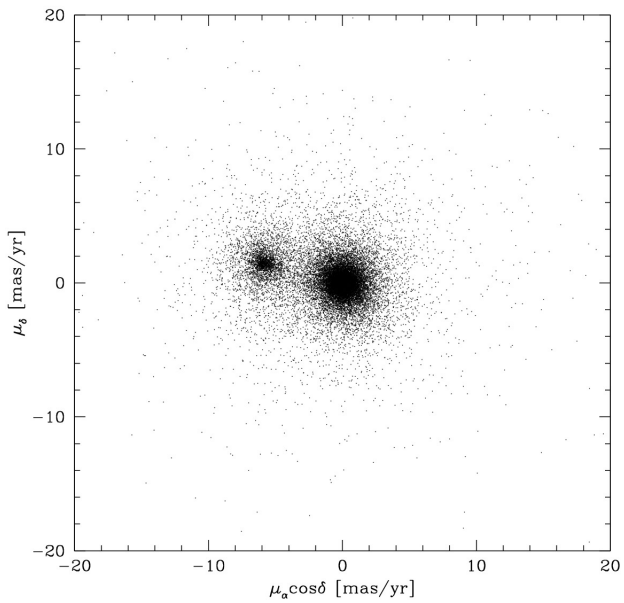


Figure A10. VPD for NGC 362.

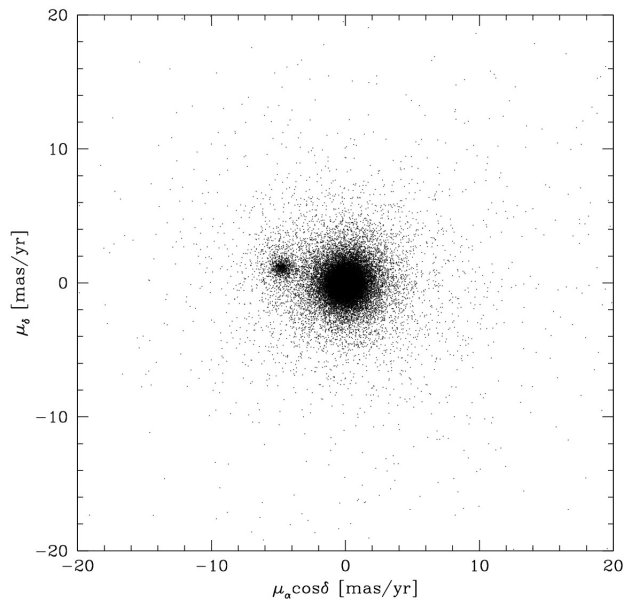


Figure A12. VPD for 47 Tuc E.

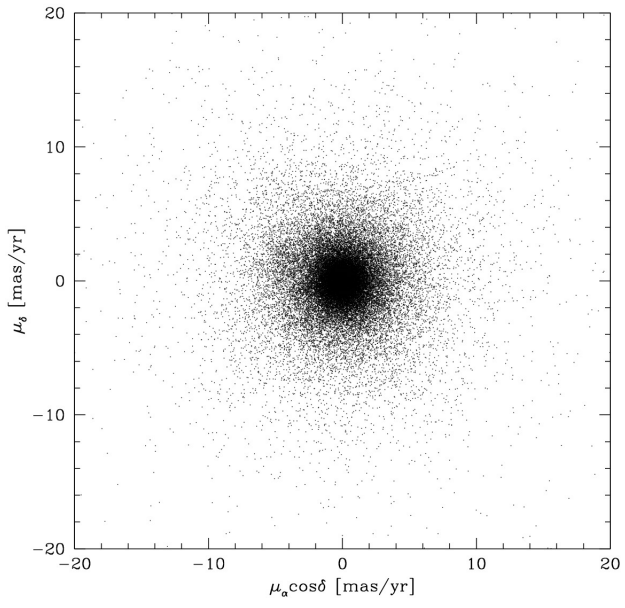


Figure A13. VPD for 47 Tuc W.